DEVELOPMENT AND INVESTIGATION OF FLUORESCENCE IMAGING PROBES

by

BAHAR SAREMI

Presented to the Faculty of the Graduate School of

The University of Texas at Arlington in Partial Fulfilment

of the Requirements

for the Degree of

DOCTOR OF PHILOSOPHY

THE UNIVERSITY OF TEXAS AT ARLINGTON

August 2019

Acknowledgements

I would like to express my heartfelt gratitude to Dr. Baohong Yuan for his guidance, and commitment throughout the course of my Ph.D studies. I am very grateful and honored to have him as my mentor and very grateful for being provided with an independent research platform in which I had the freedom of following my ideas. I learned from Dr. Yuan to always see the big picture in research and in life, and to embrace the failures as a ladder to success.

I want to thank Dr. Georgios Alexandrakis, Dr. Yi Hong and Dr. Justyn Jaworski for serving on my dissertation committee or as co-advisors. I have learned a lot about optics from Dr. Alexandrakis which has helped me tremendously in my research. I'm pleased how much Dr. Hong and Dr. Jaworski's guidance and constructive criticism lead to more profound results, by encouraging me to investigate my hypotheses deeper and more meticulously. I especially appreciate Dr. Hong and Dr. Jaworski and Dr. Liping Tang's generosity for providing their labs for polymer synthesis and measurement.

I want to thank Dr. Francis D'souza and Dr. Venugopal Bandi at the University of North Texas for their valuable collaboration and providing the environment-sensitive fluorophores.

I was lucky enough to have faculty members such as Dr. Khosrow Behbehani and Dr. Digant Dave light up my journey with their precious advice.

I was fortunate enough to have great colleagues and friends. I'd like to thank Dr. Yuan Liu, Dr. Jayanth Kandukuri, Dr. Mingyuan Wei, Dr. Binbing Cheng, Dr. Yambo Pei , Mr. Tingfeng Yao, Mr. Yang Liu and Ms. Liqin Ren, who provided a supportive and friendly lab environment.

Good friends always lift you up in the darkest moments of life. I've had great friends who were always there for me to lift me up. I want to thank all my friends for supporting me throughout my career.

I would also like to thank the Office of Graduate Studies for providing the Dissertation Fellowship, which gave me peace of mind to focus my efforts on completing this dissertation.

Last but not least, I want to thank my parents Dr. Ameri and Mr. Saremi, and my brother Navid. Although far away, their presence has always warmed my heart and given me hope and happiness. Their resilience has always inspired me and given me strength to carry on.

This work was supported in part by funding from the NSF CBET-1253199 (BY), the NHARP13310 (BY), the NIH/NIBIB 7R15EB012312-02 (BY), the CPRIT RP120052 and RP170564 (BY), and the NSF MSN 1110942 and 1401188 (FD).

August, 2019

Abstract

DEVELOPMENT AND INVESTIGATION OF FLUORESCENCE IMAGING PROBES

Bahar Saremi, PhD

The University of Texas at Arlington, 2019

Supervising Professor: Baohong Yuan, PhD.

Fluorescence imaging has attracted much attention due to high sensitivity, spatial and temporal resolution, and fast acquisition time, for imaging biomolecular processes and for diagnosis of diseases such as cancer in early stages. Fluorescence imaging in centimeter-deep tissue suffers from low spatial resolution because of the strong scattering of light. On the other hand ultrasound imaging benefits from 1000 times less scattering in the tissue and deep penetration. Ultrasound switchable fluorescence imaging is a relatively new imaging modality that combines the sensitivity of optical imaging with the depth of penetration of ultrasound imaging while preserving the resolution by only eliciting the fluorescence signal from the small focal volume of the high intensity focused ultrasound (HIFU). As such unprecedented depths can be penetrated while resolution and sensitivity of fluorescence imaging are relatively conserved.

USF imaging contrast agents directly or indirectly respond to the elevated temperatures caused by HIFU. As such thermo-sensitive USF imaging probes switch “ON” over a narrow range of elevated temperatures instantly. In this work, several different strategies for developing thermo-sensitive probes for potential use in USF imaging are studied a pH-sensitive USF contrast agent developed.

Table of Contents

List of illustrations

List of Tables

Chapter 1

Introduction

1.1 Optical imaging

Optical imaging as a sensitive imaging method, with high temporal resolution and fast acquisition time [1] has attracted attention for studying the bio-molecular processes and pathophysiological conditions such as cancer. The sensitivity of optical imaging is partly due to the contrast agents and molecular imaging probes, with detection limits of as low as picomolar to femtomolar concentrations, and signal-to-noise (SNR) ratios that surpass other imaging methods [2].

Despite all the advantages of optical imaging and its subset fluorescence imaging, imaging in centimeter-deep tissue is limited due to the turbid nature of tissue. In turbid media light would go through scattering and absorption events before being collected from the tissue [3]. For characterizing tissue certain parameters are defined: μ_a is defined as the absorption coefficient, describing the probability of absorption of light per unit distance (cm^{-1}), μ_s as scattering coefficient defining probability of scattering per unit distance (cm^{-1}), $g = \langle \cos \theta \rangle$, the average of the scattering angles, as the anisotropy of the scatter. Although g can assume values from two extreme conditions of -1 (total backward scattering) to 1 (total forward scattering), tissue scattering is often anisotropic and g is usually about 0.7 to 0.9 [4]. Based on these parameters reduced scattering coefficient is defined as $\mu_{s'} = \mu_s (1-g)$, and effective attenuation coefficient $\mu_{eff} = (3 \mu a (\mu a + \mu_{s'}))^{1/2}$). Inevitably, on average, attenuation of light in the visible spectrum about 10 fold per centimeter of tissue [2] ,posing serious limitations on the depth of penetration of optical imaging and on resolution when imaging is conducted in deep tissue.

1.2 Strategies for deep imaging

To image deep tissue, strategies to decrease light attenuation in tissue due to absorption and scattering have been undertaken. One such strategy has been choosing wave-

lengths in the three so-called “optical windows” for in-vivo imaging. In these windows: 650 nm to 950 nm (NIR-I), 1000 to 1350 (NIR-II) and 1550 to 1870 (NIR-III) [5], [6], absorption of light by blood (oxygenated and deoxygenated), skin and fat are at the lowest (Figure 1.1). Since scattering becomes lower gradually as the wavelength increases in each window, and auto-fluorescence peaks at 370 nm and decreases till 700 nm [3], imaging in optical windows confers the maximum penetration that optical imaging can offer. By taking advantage of the second optical window for imaging, the maximum depth of penetration has been reported by Dang et al. as up to 8 cm of tissue by hyper-spectral and diffuse Imaging in Near-infrared” (DOLPHIN)[7].

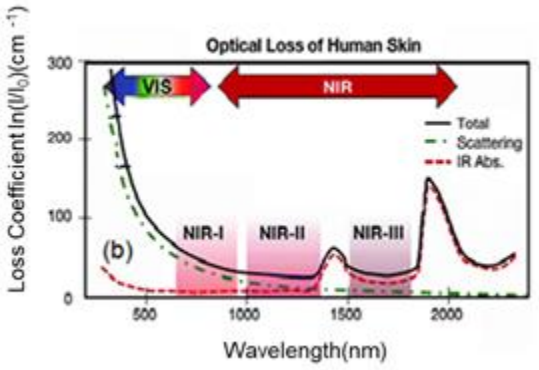

Figure 1. 1 Loss coefficient per centimeter of tissue for major tissue components in the three optical windows [5]. (Picture was incorporated with permission from the authors.)

1.3 Hybrid ultrasound and optical imaging systems

One strategy for imaging the scattering medium of tissue has been the adaptation of hybrid imaging systems that benefit from the high sensitivity and contrast of optical imaging and the high resolution and depth of penetration of ultrasound imaging at the same time [8]. Ultrasound scattering in tissue is 2-3 orders of magnitude lower than light scattering [8]. On the other hand the resolution of ultrasound is defined as (adding some references):

$$\text{Axial resolution} = \lambda \,(\#\text{ of cycles in one pulse})/2$$

Where λ is the wavelength [9],[10]. Higher axial resolutions can be achieved by a fewer cycles

in a pulse by applying ultrasound transducers that work at higher frequencies.

On a similar note the lateral resolution is defined as (adding some references):

$$\text{Lateral resolution} = \lambda/NA$$

Where NA is the numerical aperture [10],[9]. Lateral resolution also, depends on the frequency of the ultrasound transducer, as well as numerical aperture which itself depends on the geometrical dimensions of the transducer. With ultrasound transducers capable of 100 kHz to 50 MHz [9], ultrasound imaging is capable of producing a broad range of resolutions and imaging depths by itself or in a dual modality system.

1.4 Ultrasound Switchable Fluorescence (USF) imaging

In USF imaging a high intensity focused transducer (HIFU) is used to produce high localized temperature in the tissue, swiftly. USF contrast agents are sensitive to the heat produced in the focal area of the transducer. By using the USF contrast agents that switch “On” and “Off” with a sharp transition (T_{bw}) within a couple of degrees, high-resolution fluorescence imaging in centimeter-deep tissue can be achieved [11]. Choosing the fluorescent probe in the NIR region ensures that the fluorescent light can penetrate centimeters of tissue and the signal can be detected. USF contrast agents with a high I_{On}- to-I_{Off} ratio are desired to suppress the background signal coming from the I_{Off} when the probe is in the off state.

1.5 Temperature-sensitive probes

1.5.1 Temperature-sensitive fluorescent dyes

Direct thermometry with the use of temperature-sensitive fluorescent probes, has been sought after for its numerous applications. Rhodamine-B, a widely used probe for thermometry, has a mild thermo-sensitivity of 4% per degrees Kelvin when used in mixture of fluorescein-27 (FL27) and 2% per degrees Kelvin in mixture of Rhodamine-110 [12] . Advance multi-color ratiometric methods, that integrate information about two or more spectral bands ,on the other

hand, have not reached sensitivities more than 10%[12].

1.5.2 Red fluorescent proteins

Genetically encoded fluorescent proteins such as red fluorescent proteins have shown temperature sensitivity. Temperature sensitivities of E. coli expressing mRFP1, mRFP-P63A and mRFPP63A [(4R)-FP] were -1.27%, -1.26% and -0.77%/°C, respectively. Despite the negative linear relationship between the temperature and signal intensity, RFPs cannot be used in USF due to very small I_{On}/I_{Off} ratio.

1.5.3 Fluorophore-quencher-labeled microbubbles

In this method the fluorophore and quencher are attached to the surface of the microbubble. Fluorophores and fluorescence is suppressed due to the quenching of the fluorophors by the quenchers and the system is in “Off” state. After a short ultrasound pulse is applied the microbubble expands and the distance between the fluorophore and quencher grows till quenching efficiency is dropped and fluorescence is revived to “On” state. Based on the work of Liu et al. 1-MHz ultrasound transducer could increase the Ultrasound-modulated fluorescence (UMF) signal from ATTO532-NHS tagged microbubbles to about ~4 times [13].

1.5.4 Förster resonance energy transfer (FRET) (Based on linear thermo-responsive polymers)

In this method the branched linear thermo-responsive polymer (PNIPAm) is produced and then fluorophores are conjugated to the functionalized linear polymer. Conjugation happens by either NHS-fluorophore reacting with the amine functionalized polymer or by the fluorophores containing amine groups reacting with the carboxyl functionalized polymer. The fluorophores consist of FRET donors and acceptors. The donors are excited by visible light and the acceptors emit light in the Red/NIR by Förster resonance energy transfer from the donors. The energy transfer, however, being distance dependent, only takes place when the temperature is over

the lower critical solution temperature (LCST) and the linear polymer assumes a global shape in which donors and acceptors are in close proximity and FRET is feasible. For a DBD-ED and Sq660a pair in the study done by Cheng et al. with an excitation wavelength of 470 nm and emission of 609 nm depending on the co-monomers added to the polymer, I_{On}/I_{Off} between 5.3 to 7 was calculated while T_{On}/T_{Off} (Lifetime of On to Off ratio) was calculated from 1.4 to 3.3 ns [14].

1.5.4 Polarity sensitive probes: Charge Transfer Pathways (Photo-induced Electron Transfer (PeT), Internal Charge Transfer (ICT), etc.):

If the donor and acceptor are connected through a π-system so that the π-orbitals can overlap from the donor to the acceptor, upon excitation, a significant dipole, is generated through charge transfer known as internal charge transfer (ICT). In a photo-induced electron transfer (PeT) system, however, the donor and acceptor are connected with a spacer, and quenching in the excited state takes place after a redox reaction in which the donor is oxidized and the electron is transferred to acceptor [15]. This is the basis for polarity sensitive probes that act as switchable fluorescent probe (SFP). In such system, the heat generated from the high-intensity focused ultrasound (HIFU), would increase the temperature of the tissue at the focus of the ultrasound, to above the lower critical solution temperature (LCST), and elicit response from a thermo-responsive polymer. The shrinkage of the nanoparticle would affect its water content and consequently decrease the polarity of the immediate micro-environment of the dye. This would trigger the dye molecules to switch from an “Off” or dark state, in which they are minimally detectable to an “On” state.

1.6 Outline of the objectives

In chapter 2 a quantum dot (QD)/streptavidin-biotin/DNA/dye system is developed and the possibility of length dependent Förster resonance energy transfer (FRET) investigated based on DNA rulers with different lengths. Such a system can work as a model for future USF

imaging contrast agents that substitute thermo-responsive polymers in lieu of DNA rulers for FRET-based USF contrast agents utilizing quantum dots.

In chapter 3, thermo-responsive probes that utilize polarity sensitive fluorescent molecules in conjunction with thermo-sensitive polymers are studied and a set of aza-BODIPY and structurally similar dyes are introduced and their fluorescence lifetime and intensity studied while the polarity and viscosity of the microenvironment changed and the mechanism leading to such behavior investigated.

In chapter 4, both pH- and temperature-sensitive contrast agents are developed, for possible application as USF imaging contrast agents in the future. Since many illnesses from cancer to autoimmune disease are correlated with a change in the pH, such agents can be used for early detection of cancer and other life threatening conditions.

*** This chapter has been previously published in the Journal of Biomedical Optics as : Re-evaluation of biotin-streptavidin conjugation in Förster resonance energy transfer applications[15].

Chapter 2

Fluorescence Switching by Förster Resonance Energy Transfer: Re-evaluation of biotin-streptavidin conjugation in FRET applications

2.1 Introduction

Förster resonance energy transfer (FRET) is an optical phenomenon in which an excited donor molecule can transfer its energy to an acceptor molecule to emit fluorescence photons at the acceptor emission wavelengths. The transfer efficiency has been found highly dependent upon the donor–acceptor distance. Therefore, FRET has been commonly used as a tool for investigating inter- or intramolecular distance at a level of nanometers [16],[17].

To efficiently observe FRET, donors and acceptors are usually linked via various conjugation structures, such as amine-carboxyl reaction, thiol bonding, and bioaffinity binding [18],[19],[20] . Among numerous bioconjugation structures, streptavidin (SA)–biotin binding has been widely used because of its high affinity and specificity, facile nature, and commercial availability [21],[22],[23]. For example, dye-labeled biotinylated DNA molecules (biotin–DNA–dye) have been attached to a streptavidin-coated quantum dot (QD–SA) for FRET-based biomedical imaging [24] and sensing [23],[25],[26],[27]. In the structure of (QD–SA)–(biotin–DNA–dye), QD and dye serve as a donor and an acceptor, respectively. Two major advantages of this system are the large quantum efficiency of the QD and the capability of controlling the donor–acceptor distance by varying the number of bases (single-stranded) or base pairs (double-stranded) of the DNA molecule (and, therefore, the length of DNA).

Studies have observed distance-dependent FRET between the QD and the dye when changing the number of the DNA bases (or base pairs) [28], and also utilized FRET data for single-molecule sensing [27] and quantitative analysis of inter- or intra-molecular distance [28],[29],[30]. These results led to an assumed architecture for the (QD–SA)–(biotin–DNA–dye) system, which stated that “the dye acceptors on the DNA will be located at a uniform set of centro-symmetric distances from the central QD [19], [31] ” Based on this model, the FRET should depend on the DNA length or base number (or base pairs). However, a recent study found a contradictory result. In the study, the FRET was found independent of the number of DNA base pairs, if the (QD–SA)–(biotin–DNA–dye) system was adopted in PBS solution [31],[19] . Therefore, a conclusion was drawn in the study that the (QD–SA)–(biotin–DNA–dye) system might have very different architecture compared with the initially assumed one. A new architecture model for the (QD–SA)–(biotin–DNA–dye) system was proposed based on the fact that each streptavidin has four biotin binding sites. This new structure proposed that some biotinylated DNA molecules might radially extend outward from, and others tangentially attach onto, the streptavidin-coated QD surface (see Fig.5 [31]). The latter caused that some dyes might always be in close proximity to the QD surface so that the FRET became independent of the DNA base pairs. Thus, the authors questioned the use of SA–biotin conjugation for linking a QD and DNAs for distance-dependent FRET applications [31],[19] .

To further understand the (QD–SA)–(biotin–DNA–dye) system, a different perspective (i.e., ionic strength) was Investigated. Obtained data showed that the contradictory results in previous publications might be caused by the chemical–physical microenvironment of the DNA molecules as a result of the adoption of different buffer solutions (such as borate, Tris, PBS, and TE buffers). Therefore, the SA–biotin conjugation in FRET applications under varying ionic strength conditions was reevaluated. The finding in the current work reveals that the controversial results between length-dependent and -independent FRET is mainly attributed to

the ionic strength of the adopted buffer solutions. Accordingly, it was conclude that the system of (QD–SA)–(biotin–DNA–dye) is appropriate for investigating distance-dependent FRET, if appropriately selecting buffer solutions.

2.2 Materials and methods

2.2.1 Materials

Streptavidin-coated Quantum Dots (QDs): The streptavidin-coated QDs (QD655–SA, peak emission: 655 nm) were purchased from Life Technologies (Grand Island, NY, USA). The QD655–SA are expected to be 15–20 nm in size, each functionalized with 5–10 streptavidin molecules according to the production information provided by the vendor (www.lifetechnologies.com). Biotinylated Oligonucleotides Labelled with Alexa Fluor 750: In total, six strands of 3'-biotinylated oligonucleotides (10, 25, 32, 40, 50, and 70 bases) and one additional strand of non-biotinylated oligonucleotide (50 bases) were obtained from Integrated DNA Technology Inc. (Coralville, IA, USA). All oligonucleotides were labelled with Alexa Fluor 750 (NHS ester) at the 5' end. The sequences of the oligonucleotides were: (1) 5-/5Alex750N/CAA CAATAC A/3Bio/-3; (2) 5-/5Alex750N/CAA CAATAC ATC ATC TAC CAT CAT C/3Bio/-3; (3) 5-/5Alex750N/CAA CAATAC ATC ATC TAC CAT CAT CCA ACA AT/3Bio/-3; (4) 5-/5Alex750N/CAA CAATAC ATC ATC TAC CAT CAT CCA ACA ATA CAT CAT C/3Bio/-3; (5) 5-/5Alex750N/CAA CAATAC ATC ATC TAC CAT CAT CCA ACA ATA CAT CAT CTA CCATCA TC/3Bio/-3; (6) 5-/5Alex750N/CAA CAATAC ATC ATC TAC CAT CAT CCA ACA ATA CAT CAT CTA CCATCA TCC AAC AAT ACA TCA TCT ACC A/3Bio/-3; (7) 5-/5Alex750N/CAA CAATAC ATC ATC TAC CAT CAT CCA ACA ATA CAT CAT CTA CCATCA TC/-3.

Buffer Solutions: The QD's incubation buffer (2% w/v BSA in 50 mM borate buffer, pH 8.3, containing 0.05% sodium azide) was purchased from Invitrogen, denoted as borate buffer. Phosphate-buffered saline (PBS) packs (8 mM sodium phosphate, 2 mM potassium phosphate,

0.14 M NaCl, 10 mM KCl, pH 7.4) were purchased from Thermo Scientific (Rockford, IL, USA). Tris (hydroxymethyl) aminomethane (Tris) was obtained from Bio-Rad Laboratories, Inc. (Hercules, CA, USA). Tris buffer (10 mM Tris, adjusting pH to 8.0 with 1 M HCl) was prepared and used in the experiments. A TE buffer (10 mM Tris and 1 mM EDTA pH 7.5,) was purchased from USB Corporation (Cleveland, OH, USA). Two percent BSA (weight–volume ratio) were added into PBS, Tris, and TE buffers when used for conjugation.

2.2.2 Methods

2.2.2.1 Sample preparation: Samples in the present work were prepared through three steps: conjugation between QD–SA and Biotin–DNA–dye, separation of free biotin–DNA–dye from the conjugates, and dilution of the conjugates (see details in the Experimental section). Note that the buffer for conjugation was denoted as “C-buffer” and, thereafter, the buffer used to dilute the sample (by 30-fold in volume) prior to measurement as “D-buffer.”

A general procedure for sample preparation is described as follows. In 100 µL of C-buffer, 1 pmol of QD655–SA was mixed with 10 pmol of BOAF. The sample was placed on the shaker (ThermoScientific, Asheville, NC, USA) at ~6000 rpm for 45 minutes at room temperature. After conjugation, to remove the unbound DNA molecules, the sample was filtered using a 100K molecular-weight-cut-off centrifugal filter (DNA FastFlow Device, purchased from EMD Millipore Ltd., Billerica, MA, USA) at 4000 g for 20 minutes. The filtered sample was collected at 7000 g for 3 minutes according to the manual. The resulting sample was diluted to 3 mL with the D-buffer.

2.2.2.2 Fluorescence lifetime measurement: A custom-built fluorescence lifetime measurement system was employed to measure the change in the donor’s and acceptor’s lifetimes caused by FRET (Figure 1). A nitrogen laser and a pumped-dye laser (nitrogen laser: OL-4300, dye laser: OL-401, both from Optical Building Blocks Corporation, Birmingham, NJ)

were used to generate a light pulse at 490 nm, with a pulse width of ~800 picoseconds, using the OD 481 dye (Optical Building Blocks Corporation, Birmingham, NJ, USA). Collimation of the laser beam was achieved using two lenses (L1 and L2, AC254-030, Thorlabs Inc., Newton, NJ, USA). The intensity of the laser beam was controlled by a rotational neutral-density filter (Thorlabs Inc., Newton, NJ, USA), and a third lens (L3, A230TM-A, Thorlabs Inc., Newton, NJ, USA) was used to couple the beam into a 200 µm multimode optical fiber (FT200EMT, Thorlabs Inc., Newton, NJ, USA). A laser beam from the fiber was then collimated through a lens (L4, A230TM-A, Thorlabs Inc., Newton, NJ, USA) to excite the sample.

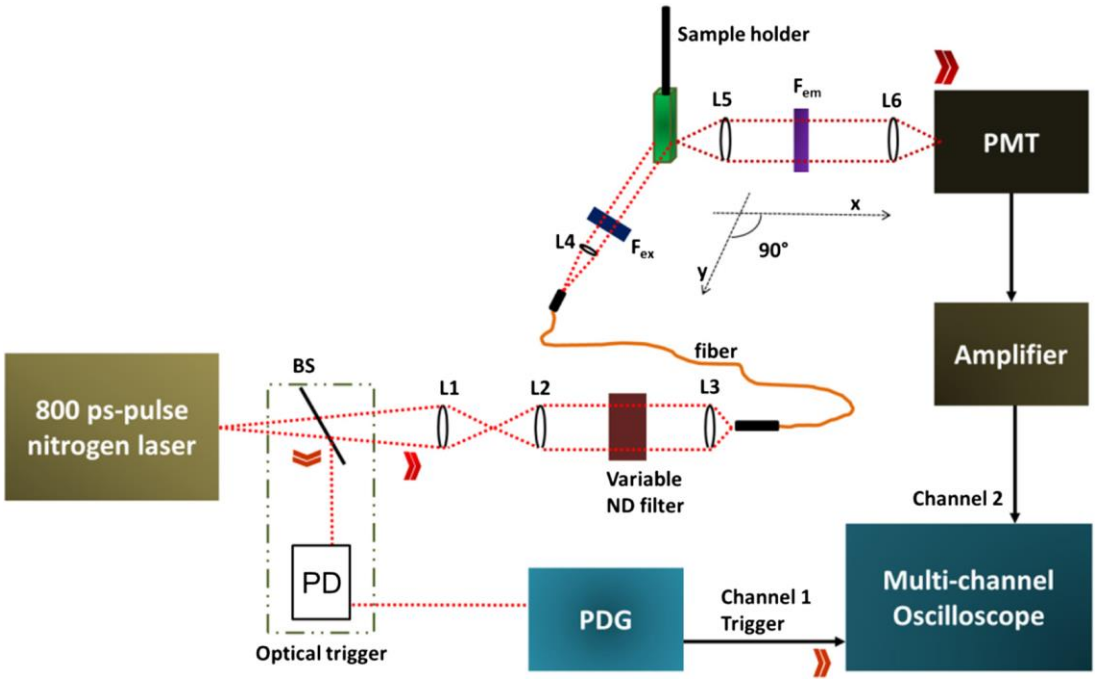

Figure 2. 1 A schematic diagram showing the fluorescence lifetime measurement system. Fex, excitation filters; Fem, emission filters; L, lens; PMT, photomultiplier tube; BS, beam splitter; PD, photodiode; PDG, pulse-delay generator; and ND filter, natural density filter[15] .

The spectral overlap of the donor (QD655) and the acceptor (Alexa Fluor750) as a FRET pair is shown in Figure 2.2. The overlap between the QD655 emission (solid blue line) and the AF750 excitation (the dashed red line) spectra can be clearly seen, which is not

significant but acceptable. The relatively small spectral overlap between QD655 and AF750 may lead to relatively small FRET efficiency. However, this can be easily compensated by the sensitive detection system and the averaging method via multiple measurements.

In this experiment, the FRET signals have been measured clearly and stably, while the donor's bleed-though was kept at the minimum. A band-pass filter with a central wavelength of 485 nm and a bandwidth of 20 nm (FF02-485/20, Semrock, NY, USA) was placed immediately after the lens to further clean the laser spectrum. Three neutral-density filters (OD 0.3, 0.4, and 0.6, Edmund Optics Inc., NJ, USA) were attached to the aforementioned band-pass filter only when measuring the QD655 emission to prevent the PMT from possible saturation as a result of the much stronger fluorescence emission from QD655 than from AF750. The emission filters for AF750 and QD655 are a band-pass filter with a central wavelength of 785 nm and a bandwidth of 62 nm (FF01-785/62, Semrock, NY, USA), and a band-passed filter with a central wavelength of 650 nm and a bandwidth of 60 nm (FF01-650/60, Semrock, NY, USA), respectively. A filter wheel (CFW-6, Thorlabs Inc., Newton, NJ, USA) was used to switch between the two emission filters. A pulse energy meter system (J-10MT-10KHZ EnergyMax sensor or J-10Si-HE Quantum EnergyMax sensor with the Labmax-Top laser power/energy meter, Santa Clara, CA, USA) was used to measure the laser pulse energy. The emitted fluorescence photons were detected by a photomultiplier tube (PMT, H10721-20, Hamamatsu, Japan). A broadband preamplifier (C5594, bandwidth from 50 kHz to 1.5 GHz, Hamamatsu, Japan) was used to convert the output of the PMT to a voltage signal and further amplify the signal. The voltage signal was then acquired by a multichannel and broadband oscilloscope (DPO 7254, 2.5 GHz, Tektronix, OR, USA). The laser pulse was coupled into a 20-meter long optical fiber (FT200EMT, Thorlabs Inc., Newton, NJ, USA) to generate an optical delay of about 100 ns, which gave sufficient time to the electronic devices to respond for best synchronization between fluorescence emission pulses and data acquisition.

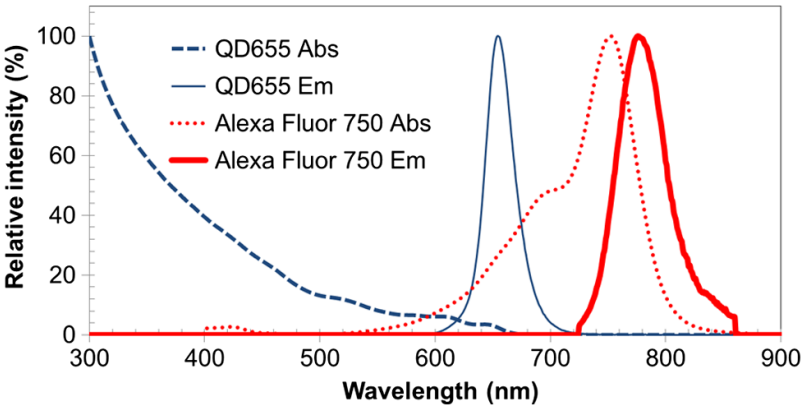

Figure 2. 2 Plot showing the spectral overlap of the donor (QD655) and the acceptor (Alexa Fluor 750) as an FRET pair [15].

An optical trigger device was placed between the laser system and the fiber coupling system to split a small amount of the excitation light from the laser and generate a voltage pulse via a fast photodiode. This voltage pulse was used to trigger a digital pulse-delay generator (PDG, DG645, Stanford Research Systems, CA, USA) and further trigger the oscilloscope for data acquisition. This setup provided very high accuracy of the synchronization between the fluorescence pulse and data acquisition, and therefore a large amount of fluorescence pulses can be acquired and averaged to improve the signal–noise ratio. Each emission decay pulse recorded from the oscilloscope used for calculating fluorescence lifetime was an average of 100 times excitation events. For each sample, the experiment was repeated at least two times (therefore the total number of the average is equivalent to 200 at least). The mean and standard derivation (std) are calculated for each sample and shown on the figures (i.e. mean ± std). Each sample was diluted to 3 mL and injected into a quartz cuvette (Starna Cells, Atascadero, CA, USA) that was fixed perpendicularly to the path of the laser beam.

2.2.2.3 Fluorescence lifetime calculation: The system impulse response function (IRF) was measured and used to deconvolve the acquired fluorescence decay data. The processed data were fitted to a single exponential decay function, using Matlab (Natick, MA, USA). The fitting was done by an iterative numerical procedure until the best agreement with the experimental decay curve was achieved.

AFM measurement: A 100 µL aliquot of each of the conjugated 70-base B2T and B2P samples were deposited on a biotinylated coverslip, purchased from Microsurface, Inc. (#Bio_02, Englewood, NJ, USA) and kept in a humidified chamber at room temperature overnight. The resulting coverslip was rinsed three times with the same D-buffer (Tris for B2T and PBS for B2P), shaking (~2000 rpm) for 3 minutes, and dried in the desiccator with vacuum. The measurement was performed with a Park XE70 AFM (Santa Clara, CA, USA), using non-contact mode with ACTA probe. At least 10 locations were selected to measure each sample. “The root mean square (RMS) of the image roughness was calculated since it is a commonly used parameter in AFM to quantify the height, which is more sensitive to peaks and valleys than the average roughness [32] .”

The system of (QD–SA)–(biotin–DNA–dye): As mentioned in Ref.[31], two possible binding modes might exist between a biotinylated DNA and a streptavidin attached on a QD: standing-up and laying-down (Figure 3-A). Significant FRET independent of the number of DNA base pairs was observed and attributed to the possibility of the laying-down binding mode. In this mode, the acceptors labeled on the DNA chains would stay within a much tighter area around the QD donor than they would in the standing-up mode (see Figure 3-A).

After an intensive investigation, however, the conclusion was suspected because the model did not take into consideration the steric hindrance from the adjacent streptavidins and the QD. The existence of the neighboring streptavidins on the QD might greatly reduce the

possibility of the laying-down binding mode because the space between each two adjacent streptavidin molecules may be limited for the fitting of DNA or oligonucleotide. Instead, we found that the observed base pair–independent FRET should be attributed to buffer ionic strength that could significantly affect the FRET of the (QD–SA)–(biotin–DNA–dye) system.

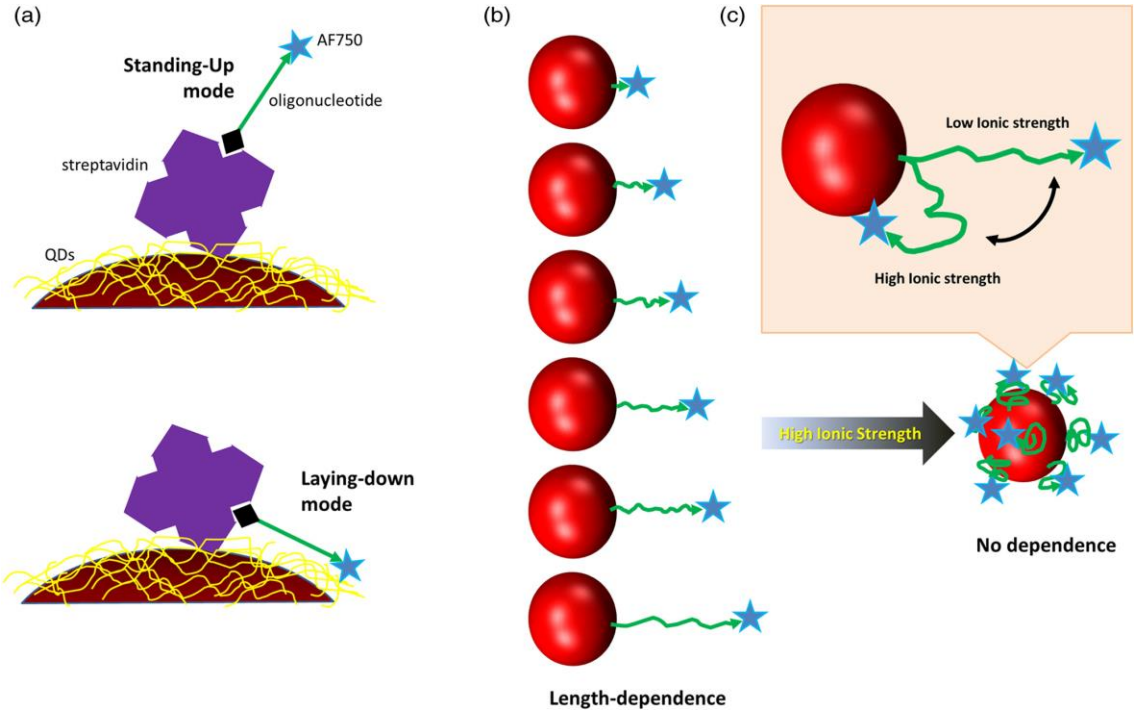

Figure 2. 3 (a) Illustration of two binding modes of biotinylated oligonucleotide to streptavidin-coated quantum dots (QDs). Not to scale. (b and c) Illustration of the hypothesis in this work. At low-ionic strength, oligonucleotide stretches from the QDs, leading to length-dependent FRET. At high-ionic strength, oligonucleotide is more flexible but is prone to bending toward QDs. The separation distance between donor and acceptor becomes smaller, falling well into the FRET range, so that no length-dependent FRET was observed [15].

Streptavidin-coated QD655 (QD655–SA) was selected as a donor in this study, which has a structure similar to QD609–SA used in Ref.(16) with a longer peak emission wavelength (655 nm). A near-infrared (NIR) fluorophore, Alexa Fluor 750 (AF750), was adopted as the acceptor based on the reasonable spectral overlap with the QD655–SA donor (see Figure 2.2). While a biotin was attached to the 3' end of an oligonucleotide (a single-stranded DNA), the fluorophore of AF750 was labeled at the 5' end. The AF750-labeled biotinylated oligonucleotide was denoted as BOAF.

Six oligonucleotides with base numbers of 10, 25, 32, 41, 50, and 70 were adopted (see details in Experimental section). After conjugation, a QD655–SA~BOAF structure was formed. While the bindings of biotin to streptavidin occur in the C-buffer, the oligonucleotide conformation (stretched or coiled) depends on the D-buffer. It is reasonable to hypothesize that the donor–acceptor distance will correlate with the base number of BOAF if the standing-up binding mode is dominant and the oligonucleotide is in the stretched conformation (see Figure 2.3-B). Therefore, the measured FRET (indicated by the AF750 lifetime in this study) will depend on the base number of the oligonucleotide.

Whenever the oligonucleotide transits from the stretched to the coiled structure as a result of the change of the D-buffer, the donor-acceptor distance and thus the FRET will lose the correlation with the base number (see Figure 2.3-C). By contrast, if the laying-down mode is dominant the FRET will not (or very weakly) correlate with the base number, no matter the conformation of the oligonucleotide and the composition of the buffers.

To characterize the FRET event, the fluorescence lifetimes of both the acceptor AF750 and the donor QD655 were measured with a customized instrument (see the previous section for details). Compared with intensity, the fluorescence lifetime is insensitive to the errors caused by unknown fluorophore concentration variation, and is therefore more reliable. A molar ratio of

QD655–SA to BOAF at 1 pmol/10 pmol was employed in the present study. Since each QD has 6–10 streptavidin molecules according to the provided information from the vendor, Invitrogen, the molar amount of streptavidin is 6–10 pmol. Consequently, the biotin–streptavidin ratio in this study was ~1–1.67. Such a relatively low ratio has the following advantages: (1) it can reduce the possibility of multiple BOAFs binding on one streptavidin; and (2) thus the effect of acceptor concentration on the FRET is minimized and the donor–acceptor distance is the major factor affecting the FRET.

2.3 Results and discussion

2.3.1 Fluorescence lifetime calculation

A tail fitting strategy was adopted to maximally remove two possible noises: (1) the laser leakage and (2) the emission from the acceptors (AF750) that are directly excited by the laser. The raw decay curve was truncated after an inflexion point and then data-fitting via a single exponential function was performed. As an example, Figure 2.4 shows the step by step process for the 25 base Borate(C-buffer) to Tris (D-buffer) sample.

The cutting point was selected based on the original decay curve. The lifetime was fitted by using the data after the cutting point. Remember that both the laser leakage and the direct excitation of the acceptors decay much faster than the FRET signal. Therefore, the head part of the decay curve is the data that is possible to be contaminated by the two types of noise.

The cutting point was selected based on the original decay curve. The lifetime was fitted by using the data after the cutting point. Remember that both the laser leakage and the direct excitation of the acceptors decay much faster than the FRET signal. Therefore, the head part of the decay curve is the data that is possible to be contaminated by the two types of noise

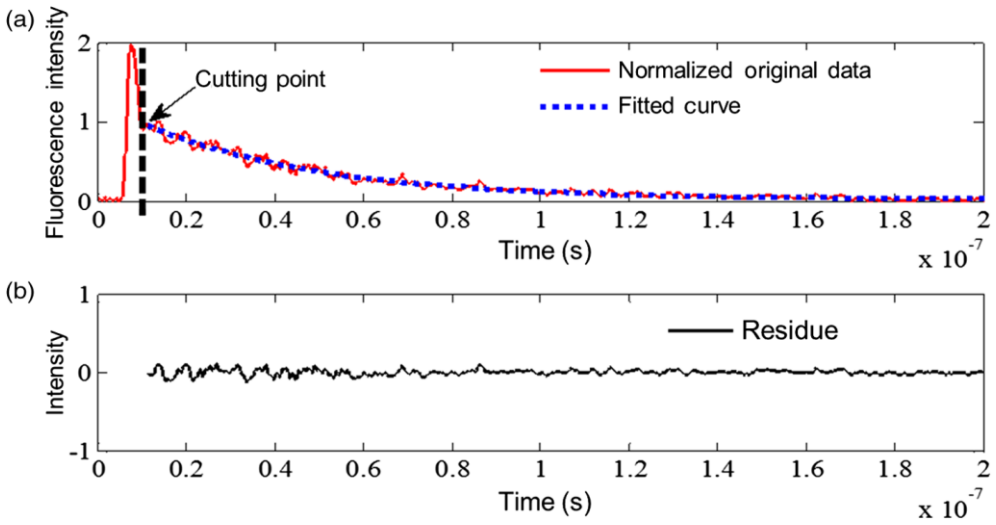

Figure 2. 4 Fluorescence lifetime calculation method. (a) Illustration of the decay curve for 25-base BOAF with borate as C-buffer and Tris as D-buffer and a single exponential tail fitting by setting a cut-off point. (b) Residues are shown versus time.2.3.2 Effect of buffers (ionic strength) on FRET:

When borate was used as C-buffer and Tris as D-buffer, for oligonucleotides with 10 bases, the fluorescence lifetime of the acceptor AF750 was found to be 36.9± 0.59 ns (Figure 2.5-A), which was significantly longer than the natural fluorescence lifetime of AF750 (~0.7 ns) [33]. There exists documented evidence that the lifetime of the acceptor increases in a FRET system[34],[35] , although it has been studied less rigorously than the increase of the donor's lifetime. On the other hand, the average lifetime of the donor QD655 for all the bases was measured to be 38.8 ns (Figure 2.5-B), consistent with the value given by the manufacturer (~30–40 ns). However, it should be noticed that the donor's lifetime decreased when the acceptor (AF750)-labeled 10-base DNA linker was used. The lifetime of QD is decreased from 38.8 ns to 34 ns in Tris, while from 38.8 ns to 32 ns in PBS (Figure 2.5-B). The result indicated an obvious FRET occurrence between QD655 and AF750. The lifetime reduction of the donor (from 38.8 ns to 32 or 34 ns) is not as significant as the lifetime lengthening of the acceptor

(from < 1 ns to >35 ns). This is mainly attributed to the following factors: (1) the relatively low (~10) acceptor per donor ratio (APD) in the conjugation step; (2) significantly higher extinction coefficient and quantum yield of the donor (QD655) compared to the acceptor (AF750). The above factors contribute to the observation that the the donor's lifetime had not been significantly affected by the acceptors.

Apparently, the lifetime of AF750 in QD655–SA~BOAF was found to gradually decrease as the base number increased, as shown by the purple curve with filled squares in Figure 2.5-(a). When the base number is greater than 50, no significant change in the lifetime of AF750 is observed, which indicates that acceptors may be out of the FRET range and/or the background fluorescence is dominant. The observed lifetimes of 16.7±1.82 ns and 14.9±4.63 ns for the 50 and 70 bases samples could be partially attributed to the background fluorescence noise (see the following section of Background noise of fluorescence). Therefore, the length-dependent FRET was observed in the system of QD655–SA~BOAF.

This result provides strong evidence for this hypothesis of the dominant standing-up mode in Figure 2.3-(a). Figure 2.5(b) shows that the lifetime of the donor QD655 is relatively stable for all oligonucleotide sequences (with an average lifetime 38.8 ns and varying within a range of ±4.4 ns). This is mainly attributed to the fact that the ratio of acceptor–donor was relatively low in the conjugation and that the donor's lifetime had not been significantly affected by the acceptors.

Interestingly, the length-dependent FRET loses when the Tris is replaced with PBS as the D-buffer (the brown curve with solid triangles in Figure 2.6(a). The lifetimes of AF750 at 50 and 70 bases significantly increases compared with those measured in the Tris buffer. The lifetime fluctuates when the base increases (in a range of ± 6.1 ns with an average of 35 ns), suggesting large FRET occurring.

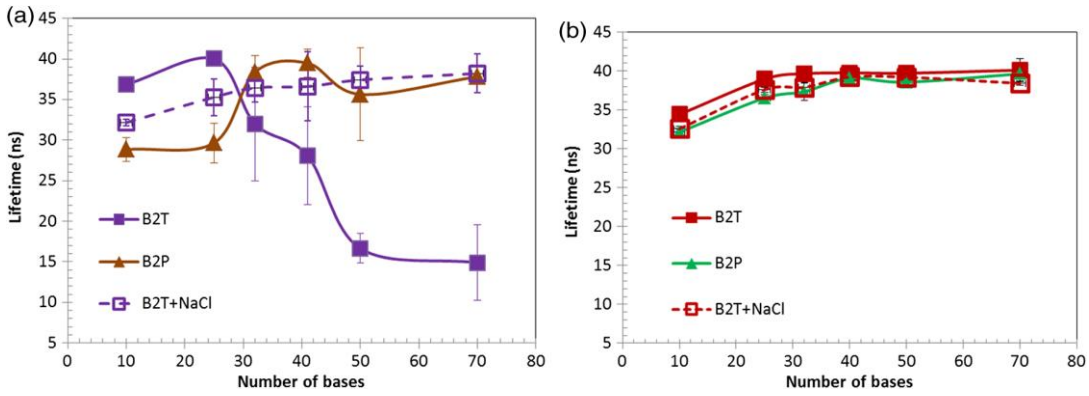

Figure 2. 5 Fluorescence lifetimes of (a) the acceptor AF750 and (b) the donor QD655-SA vary as the base number of oligonucleotide increases. Excitation: 490 nm; emission: 785⁄62 nm bandpass filter for (a) and 650⁄60 nm bandpass filter for (b). B2T: the sample was incubated in borate buffer and then diluted with Tris buffer. B2P: the sample was incubated in borate buffer and then diluted with PBS buffer. B2T + NaCl: 140 mM NaCl was added into the B2T sample [15].

This result implies that the length-dependent FRET is favorable in relatively low ionic strength buffer (borate and Tris, 10 mM) as opposed to the length independence in a relative high-ionic-strength buffer (PBS, 162.7 mM). To further investigate the effect of ionic strength on the length-dependent or -independent FRET, we implemented a straightforward experiment of adding c.a.140 mM NaCl to the B2T samples (C-buffer: borate; D-buffer: Tris), and measuring the lifetime of AF750 again. As shown by the dashed purple curve with open squares in Figure 2.5(a), the lifetime of AF750 loses the length-dependence that is originally observed in the Tris buffer and remains a relative stable value for all oligonucleotide sequences (with an average of 36.5 ns and varies within a range of ± 3.6 ns). This length-independent FRET resembles the result observed in PBS buffer.

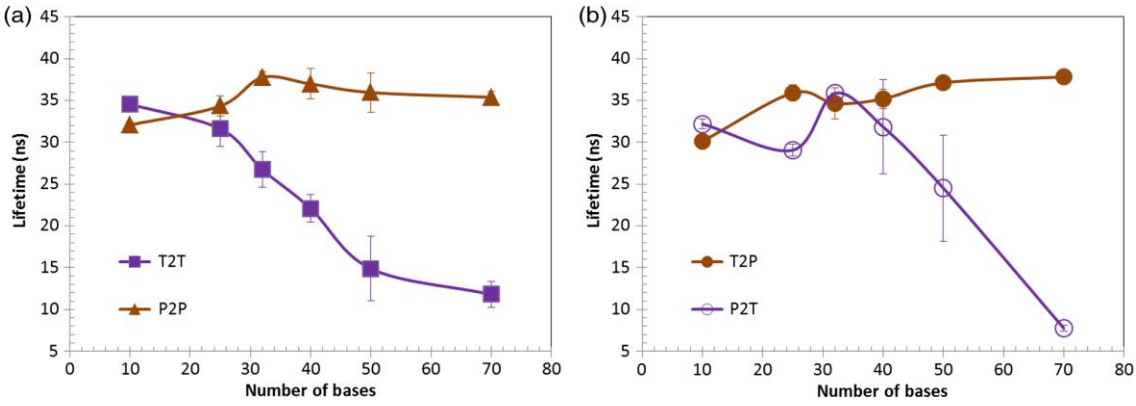

Figure 2. 6 Fluorescence lifetimes of the acceptor AF750 in QD655–SA~BOAF with varying base numbers in different buffer solutions. T2T: the samples were conjugated in Tris buffer and then diluted with Tris buffer. P2P: the samples were conjugated in PBS buffer and then diluted with PBS buffer. T2P: the samples were conjugated in Tris buffer and then diluted with PBS buffer. P2T: the samples were conjugated in PBS buffer and then diluted with Tris buffer. The excitation light and emission filters are the same as in Figure 2.5.

Accordingly, we conclude that the length-dependent FRET is favorable in low ionic strength buffers, such as 10 mM Tris, and unfavorable in relatively high ionic strength buffers, such as PBS or Tris+NaCl. It has been reported that oligonucleotide becomes more flexible when ionic strength increases [29],[36] . The reason is that excess cations screen the negatively charged backbone of oligonucleotide.

At low ionic strength, oligonucleotide stretches outward from the QD655–SA, leading to length-dependent FRET (Figure 2.3(b)). At high ionic strength, oligonucleotide is of high flexibility, making it prone to bend toward QD655–SA (Figure 2.3(c)) and lose the distance dependence. We also excluded the effect of pH on FRET by adjusting pH from 6.0 to 9.0 (data not shown), although the difference in pH between the Tris buffer (8.0) and the PBS buffer (7.4) used in this study was not significant. While the conformation of oligonucleotide can be altered at high ionic strength, another question is whether such conformation change will hinder the binding between BOAF and QD655–SA in the initiate conjugation step (in C-buffer).

To address this question, we investigated the lifetime change of AF750 in different combinations of Tris and PBS buffer solutions (as C- or D-buffer, or both). Note that the total volume for conjugation is 100 µL while the final diluted solution is 3000 µL (30-fold dilution). As shown in Figure 2.6(a), length-dependence of AF750 lifetime was observed for T2T sample (Tris as both C- and D-buffers), while no dependence for P2P sample (PBS as both C- and D-buffers) was found.

When the sample was conjugated in Tris and then diluted with PBS buffer (T2P), the dependence disappeared (Figure 2.6(b) brown curve with solid circles). By contrast, when the sample was conjugated in PBS and diluted with Tris buffer (P2T), the length-dependence of AF750 lifetime reappeared (the purple curve with open circles in Figure 2.6(b)).

Taken together, use of PBS as C-buffer is not able to significantly affect the binding between BOAF and QD655–SA. It is worth noting that adding 2% (weight–volume ratio) BSA into the C-buffer is necessary to maintain a good stability of QD655–SA and a relatively high viscosity of the solution for the centrifugal filtering process (see Experimental section for details). As long as the D-buffer (or the final solution) is Tris with ionic strength of ~10 mM, length-dependent FRET is observable. In fact, such low-ionic-strength Tris buffer has been widely used in the literature for investigating the DNA linked FRET system [19], [23], [25], [26], [30] . Like Tris, TE is another commonly used buffer with lower ionic strength compared with PBS. We also obtained similar results when replacing Tris with TE buffer (Figure 2.7 and 2.8).

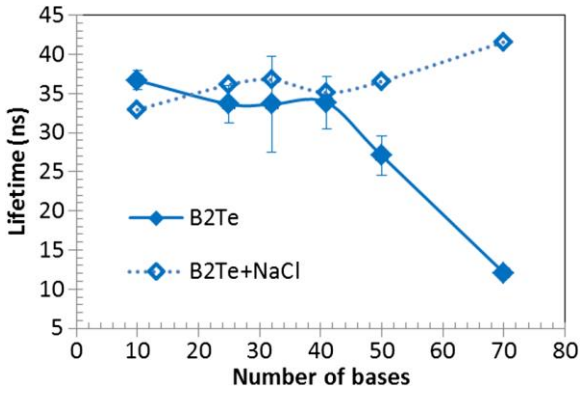

Figure 2. 7 Fluorescence lifetime of the acceptor AF750 in QD655–SA~BOAF with varying base numbers in buffer solutions of B2Te and B2Te + NaCl. B2Te: the sample was incubated in borate buffer and then diluted with TE buffer. B2Te + NaCl: 140 mM NaCl was added into the B2Te sample. Excitation: 490 nm; emission: 785⁄62 nm bandpass filter [15].

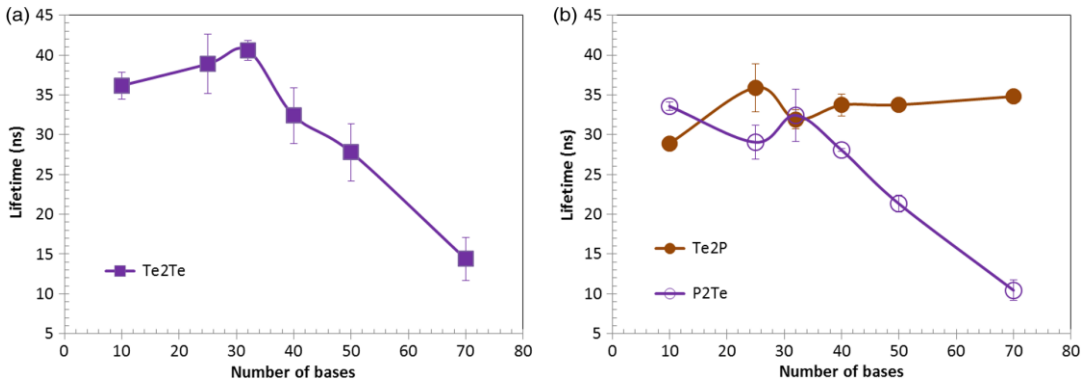

Figure 2. 8 Fluorescence lifetime of the acceptor AF750 in QD655–SA~BOAF with varying base numbers in buffer solutions of (a) Te2Te and (b) Te2P and P2Te. Te2Te: the sample was incubated in TE buffer and then diluted with TE buffer. Te2P: the sample was incubated in TE buffer and then diluted with PBS buffer. P2Te: the sample was incubated in PBS buffer and then diluted with TE buffer. Excitation: 490 nm; emission: 785⁄62 nm bandpass filter [15].

Currently, it is unclear why the samples with 10 bases do not show the highest value in the acceptor's lifetime in Figure 2.5 (A) and Figure 2.8 (A). Possible reasons may include: (1) self-quenching of acceptors may happen because the average distance between two adjacent

acceptors becomes short when the DNA base is small; (2) FRET may become saturated if the donor-acceptor distance is so short; (3) some system measurement errors may exist.

2.3.3 Background noise of fluorescence (measured from control samples)

The lifetime of AF750 with all the different lengths of the biotinylated DNA molecule along with the non-biotinylated DNA was measured in PBS, Tris and TE as a control of the acceptor's lifetime (Figure 2.9). The calculated lifetimes are <1 ns and independent of the number of bases, and close to the natural lifetime of AF at 0.7 ns.

To further evaluate the background fluorescent noise, another two control samples were adopted: (1) QD655–SA alone and (2) QD655–SA with non-biotinylated AF750-labeled oligonucleotides (50 bases). In Figure 2.10 (a), the lifetimes of the QD655–SA alone samples in B2T and B2P are shown to be 7.3±1.10 ns and 7.10±0.09 ns, respectively, when measured using the AF750 emission filter (785/62 nm). They are much shorter than the lifetime of QD655–SA alone samples (38.6±1.01 ns or 38.5±0.65 ns) in Figure 2.10 (b) when measured using the QD emission filter (655/60 nm).

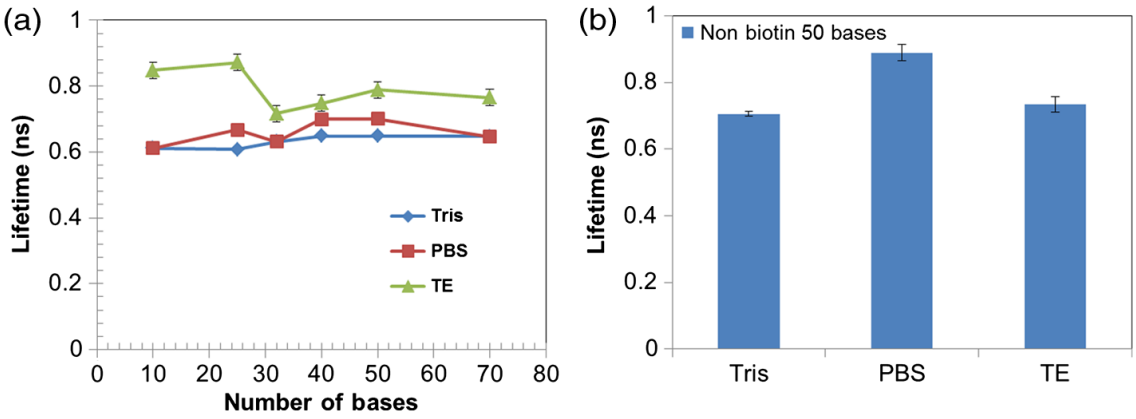

Figure 2. 9 Lifetime of Alexa Fluor 750 in Tris, TE, and PBS versus the number of DNA bases for (a) biotinylated DNA and (b) 50 bases non-biotinylated DNA [15].

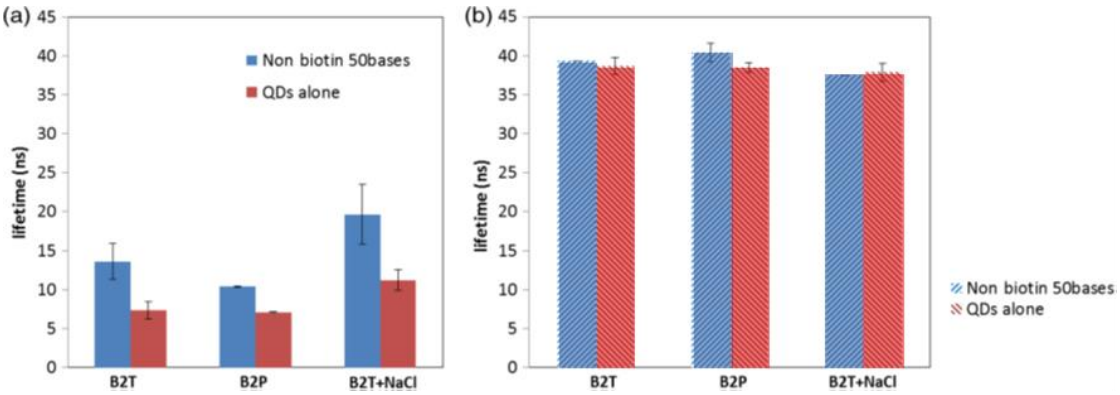

Figure 2. 10 Fluorescence lifetime at the acceptor's (a) and the donor's emission channels (b). Blue: 50-base oligonucleotide without biotin; red: QD655-SA alone. Excitation: 490 nm; emission: 785⁄62 nm bandpass filter for (a) and 650⁄60 nm bandpass filter for (b). Samples of B2T, B2P, and B2T + NaCl are the same as in Figure 2.5.

However, they are much longer than the laser pulse width (<1 ns). Therefore, these results indicate that a small amount of fluorescence can be emitted from QD655–SA itself within the spectrum band of the AF750 emission filter (so called bleed-through from the donor to the acceptor channel). It was found that the intensity of the bleed-through is usually much weaker compared with the FRET signal from the BOAF with bases <50 (remember that the fluorescence lifetime is calculated based on the emission decay curve). Accordingly, the effect of these fluorescence noises on the FRET can be ignored. Therefore, we conclude that the direct emission from QDs may be one of the dominant sources of the received photons when the measured lifetime is around or below 7.3 ns.

After the QD655–SA was mixed with the non-biotinylated AF750-labeled oligonucleotides, the same procedures as processing the biotinylated samples were followed. Compared with QD655–SA alone samples, the lifetimes in B2T and B2P increase (13.6±2.27 and 10.4±0.08 ns, respectively, see Figure 2.10 (a)). However, these two values are much larger than the natural lifetime of AF750 (~0.7 ns). This is mainly attributed to the FRET between the QD655–SA and the remaining AF750 in the solution (although the same filtering steps have

adopted, a small amount of AF750-labeled oligonucleotides may remain in the solution). This type of FRET is strongly dependent on the concentration of AF750, instead of the base numbers of the oligonucleotides. After the filtering, the amount of the remaining AF750-labeled oligonucleotide is usually small, and the intensity of this type of FRET is also much weaker than the FRET intensity from the SA-biotin conjugated samples with bases <50. Consequently, this type of FRET is not dominant until the bases are close to or above 50. Similarly, we conclude that this type of FRET may be another dominant source of the received photons when the measured lifetime is around or below 13.6 ns. On the other hand, the QD655–SA lifetime measured in the spectrum of QD655 emission filter remains stable (39.33±0.02 ns in B2T and 40.4±1.23 ns in B2P, see Figure 2.10(b)), which indicates that the remaining AF750 does not significantly change QD655 fluorescence emission properties. Similar results were found in samples where NaCl was added (see Figure 2.10(a) and 2.10(b)).

2.3.4 Discussion about using the acceptor lifetime as FRET indicator

Conventionally, when lifetime is used for FRET studies, the shortening of the donor's lifetime (instead of the lengthening of the acceptor's lifetime) is used as the FRET indictor if the donor and acceptor have comparable lifetimes, extinction coefficients, quantum yields and widths of the emission spectra. This is mainly due to two reasons. (1) Usually, the donor channel has relatively weaker bleed-through from the acceptor emission than the acceptor channel has from the donor emission. This is because the wavelength of the laser is usually close to the excitation peak wavelength of the donor but is far away from that of the acceptor, and therefore the donor emission is usually stronger than the acceptor emission. (2) The donor is less possible to be excited (and further emit light) by the emission light of the acceptor because usually there is no or ignorable spectral overlap between the acceptor emission and donor excitation spectra. In contrast, it is possible that some acceptors are directly excited (and further emit light) by the emission light of the donors because of the spectral overlap between the donor emission and

acceptor excitation spectra. This type of phenomenon can be called re-absorption-and-re-emission and is different from FRET (FRET does not involve donor emission).

However, compared with the acceptor, if the donor has a much narrower emission spectrum, a much longer lifetime, a much larger extinction coefficient, and a much higher quantum yield, the lengthening of the acceptor's lifetime can be used and may be even better as a FRET indicator [34]·[35]. This is true for the FRET system adopted in this study (QD655-DNA-AF750). The above parameters for QD655 and AF750 are listed in Table 1 for comparison.

Table 2. 1 Comparison of fluorescence parameters of the donor and acceptor studied in the current work┼, [15].

	Width of the Emission spectrum (nm)		Lifetime (ns)	Quantum yield	Extinction coefficient ($cm^{-1}M^{-1}$)
	FWHM*	FWTM**			
QD655 (Donor)	~30	~65	>35	0.6	2,900,000 at 488 nm
AF750 (Acceptor)	~54	~108	0.7	0.12	240,000 at 749 nm

┼see the data from the manufacturer: http://www.lifetechnologies.com; * Full width at the half maximum; ** Full width at one tenth of the maximum;

The concern of donor's (QD655) bleed-through to acceptor (AF750) channel can be efficiently minimized, because QD655 has a narrow emission spectrum and almost no overlap with the pass band of the emission filter of the acceptor channel. This has been validated by the control sample (i.e. the sample only with quantum dots) in which the contribution of this type of noise is weak. In addition, the effect of the fluorescence emission caused by the direct excitation of the acceptor AF750 on the FRET signal can be very easily eliminated because its lifetime <1 ns and therefore the emission decay is much shorter than the FRET based emission pulse. This type of fluorescence noise can be easily eliminated by using a time gating method to get rid of the head part of the raw data. Regarding the effect of the re-absorption-and-re-emission on

FRET, current data clearly showed that it is ignorable in the adopted QD655-DNA-AF750 system. This can be seen from the following facts. (1) If the effect of the re-absorption-and-re-emission was dominant, the acceptor lifetime should be >35 ns. However, when QD655 is mixed with non-biotin DNA-dye, the measured acceptor lifetime is between 10 and 20 ns (see the data in Figure 2.10), which is much shorter than the QD655 lifetime (>35 ns). Therefore, the measured signal should not be caused by the re-absorption-and-re-emission effect. Instead, it is mainly caused by the slight bleed-through from the QD655. (2) In Figure 2.5 and 2.7, the dependence of the acceptor lifetime on the DNA length is eliminated when adding NaCl into the sample. This fact indicates that the measured signal from the acceptor channel should not be caused by the re-absorption-and-re-emission phenomenon because this phenomenon is independent of NaCl concentration. Therefore, the effect of re-absorption-and-re-emission is ignorable. The following reasons may explain why the effect of the re-absorption-and-re-emission is ignorable in the adopted QD655-DNA-AF750: (a) both the donor and acceptor have very low concentration (1 pico mole donor and 10 pico mole acceptor) in the sample; (b) the acceptor has low quantum yield and small extinction coefficient; and (c) the spectral overlap between donor and acceptor is small.

Here we summarize and compare the possible signal components in the acceptor channel of the adopted QD655-DNA-AF750: (a) when the acceptors (AF750) are well attached on the donor (QD655) and they are within the FRET distance range, the FRET is the dominant effect; (b) when the acceptors are attached on the donor but are separated so far that they are out of the FRET distance, two possible effects may be dominant: the bleed-through from donor (QD655) to acceptor (AF750) and the FRET between the donors and those unattached free acceptors (i.e. the residue of the free acceptors, because they are free and have a small possibility to reach the vicinity of the donor); (c) the re-absorption-and-re-emission may be the weakest effect, and it does not show observable effect in these results.

In contrast, using donor's lifetime shortening as the FRET indicator has some

disadvantages. Specifically, to shorten a bright quantum dot's long lifetime (QD655>35 ns), a large amount of acceptors (AF750) is usually needed. This is because: (a) the donor (quantum dots) usually has much larger quantum yield and extinction coefficient, and much longer lifetime than the acceptor (AF750); (b) all or the majority of donors (quantum dots) should have enough acceptors (AF750) to generate obvious FRET (in contrast, if only a small portion of quantum dots are quenched by the AF750, the lifetime will not decrease significantly).

When a large amount of acceptor (AF750) is used, it can generate some problems. (a) More residue of the free AF750 (unattached DNA-AF750) may exist in the sample (although a centrifugal filter was always used to get rid of the free DNA-AF750 as much as possible). These free dyes in the sample would also shorten the lifetime of the donor (quantum dots) (but not the FRET that we are investigating). Thus, it is difficult to differentiate the effect of the free dye from the effect of the attached dye. (b) Therefore, the donor's lifetime will also depend on the acceptor concentration (the more AF750 residue in the sample gives the shorter of the donor's lifetime), which can be confused with the FRET we are investigating via the QD-DNA-dye system.

More importantly, it may not be practical to attach a large amount of acceptors on one quantum dot (donor). This is because the number of the streptavidin on each QD655 is limited ~6-10 (based on manufacturer provided data). Although each streptavidin has four biotin-binding sites, in practice it is highly possible that ~1-2 binding sites on each streptavidin are not available for biotin-DNA-AF750 because they may be blocked by the quantum dot and/or the surrounding other streptavidins due to the steric hindrance. Thus, the number of the acceptors that can be attached on one donor is <30 (3x10). Therefore, to achieve a large number of the acceptors per donor (APD) may be impractical. Thus, if a significant reduction of the donor's lifetime is found, it is highly possible to be caused by the residue of the free acceptors, which has nothing to do with FRET that we are investigated via the QD-DNA-dye system.

However, if using the lengthening of the acceptor's lifetime as the FRET indicator, the FRET efficiency is very high due to the high quantum yield and extinction coefficient of the

quantum dots. Therefore, we can maintain a small number of acceptors per donor (APD=~10), which is practically possible, and then detecting the lifetime change of the acceptor for FRET study. Thus, the residue of free acceptors (AF750) is small and the FRET is mainly depending on the donor-acceptor separation distance.

2.3.5 Further evidence from Atomic Force Microscopy (AFM).

To further verify this hypothesis, AFM was employed to investigate the attachment of the QD655–SA~BOAF (70 bases) on the surface of a biotinylated coverslip (Bio_02, MicroSurfaces Inc, NJ, USA). Since the 70 bases linker caused no FRET in low salt solutions but a dramatic FRET in high salt solutions, it was an all-or-nothing condition. Furthermore, it has a relatively long chain so that its conformation change could be possible be detected by AFM. Compared with the biotinylated oligonucleotides, the biotins on the coverslip have much smaller dimension. Thus, the steric hindrance from the surrounding SAs on the QD655 can be dramatically reduced. In addition, because of the low ratio of BOAF to streptavidin used in the present study, there are unoccupied binding sites of streptavidin in QD655–SA~BOAF. They will be possibly available for the biotin moiety on the surface of the coverslip, so that QD655–SA~BOAF may be immobilized on the surface.

As shown in Figure 2.11-A, few QD655–SA~BOAF were observed on the surface when the biotinylated coverslip was incubated with the B2T conjugated sample (10 locations were measured and compared). The RMS of the B2T sample was estimated to be 0.765 nm, which does not significantly differ from that of the original biotinylated coverslip sample (0.619 nm, Figure 2.11(C). On the contrary, the RMS value was found to increase remarkably to 1.988 nm, when incubating with the B2P sample (Figure 2.11(b)). Furthermore, the observed peak heights of the biotinylated chains on the coverslip (coated by the manufacturer) were found to be 10–18 nm (see Figure 2.11(c)). After conjugating with QD655–SA~BOAF, we found that the height values of peaks for the B2P sample increased by 15–20 nm (Figure 2.11(b)), which fits well in

the diameter range of QD655–SA, according to the vendor's manual. Because the sample was measured after the buffer solution had dried, the height contributed by oligonucleotide molecules would be hardly observed. Consequently, we conclude that much more QD655–SA~BOAFs are attached on the coverslip surface in the B2P buffer than that in the B2T buffer. This result indicates that the binding between the streptavidin on QD655 and the biotin on the coverslip was more feasible in B2P sample (with high ionic strength) than in the B2T sample (with high ionic strength).

Figure 2.11(d) shows a possible mechanism to explain the above result. For the B2T sample, the oligonucleotide molecules may be stretched-out because of the low ionic strength of the buffers (see the left panel in Figure 2.11-D). These stretched oligonucleotides may significantly reduce the possibility of the SAs on the QD655 conjugating with the biotins on the coverslip. In contrast, for the B2P sample, the oligonucleotide molecules may be significantly coiled because of the high ionic strength of the buffers (see the right panel in Figure 2.11(d)). Thus, the possibility of the SAs on the QD655 exposing to the biotins on the coverslip can dramatically increase, which leads to the immobilization of the QD655. The above result may be considered an additional evidence for verifying the hypothesis about the effect of the buffer ionic strength on the conformation change of the oligonucleotides.

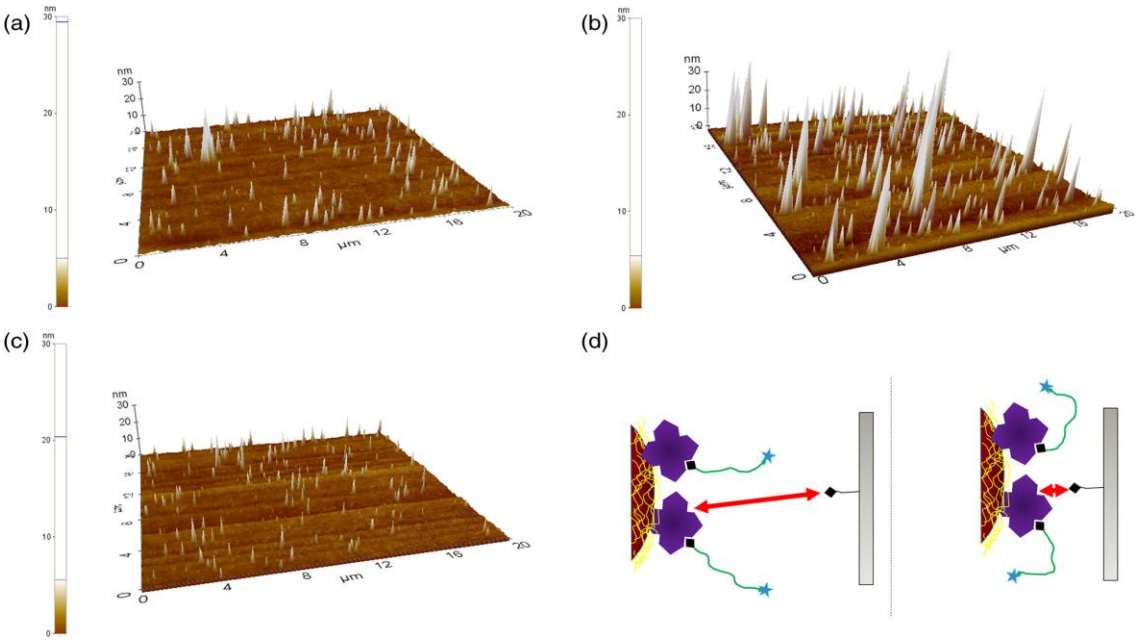

Figure 2. 11 Representative AFM images of biotinylated coverslips incubated with the conjugated solution of QD655–SA~BOAF (70 bases). (a) B2T, (b) B2P samples (note that the peak heights are not limited by the maximum z scale of 30 nm), (c) biotinylated coverslip al alone. (d) Illustration of the attachment of QD655–SA~BOAF (70 bases) on the biotinylated coverslip surface. At low-ionic strength (in Tris buffer), the available binding sites of streptavidin were blocked by stretched-out oligonucleotide molecules (left), leading to difficulty in attaching. At high-ionic strength (in PBS buffer), the binding sites were exposed (right), which facilitates the attachment [15].

2.4 Conclusion

In the buffers with low ionic strength (such as borate, Tris, and TE buffer), length-dependent FRET between QD655–SA and BOAF was confirmed by the observation of the acceptor AF750's fluorescence lifetime. In the buffers with high ionic strength (such as PBS and NaCl-added Tris), strong length-independent FRET was observed. The independence was likely attributed to the increased flexibility of the oligonucleotide chain when the cations screen the negatively-charged backbone of oligonucleotide. This flexibility increases the possibility of the terminal-attached acceptors (AF750) approaching the vicinity of the donor. If appropriately

selecting buffer solutions and the streptavidin–biotin molecular ratio, we draw the following conclusions based on the above data: (1) the system of (QD–SA)–(biotin–DNA–dye) is appropriate for investigating distance-dependent FRET between the QD and the dye if they are linked by a single-stranded DNA, and (2) the effect of the streptavidin's multiple binding modes on the FRET (proposed in Ref. [31]) may not be dominant compared with the effect of the buffer ionic strength.

*** Acknowledgements: I want to thank Dr. Mingyuan Wei for conducting the AFM experiment, and Dr. Yuan Liu for helping with the lifetime calculations and Dr. Bingbing Cheng for maintaining the laser.

Chapter 3

Exploring NIR aza-BODIPY-based and structurally-related polarity sensitive probes with ON-and-OFF fluorescence switching

3.1 Introduction

Fluorescence imaging is a sensitive and non-invasive method for investigating physiological and bio-molecular processes in vitro and in vivo. Tuning the excitation light to 650-900 nm (red-NIR) has made fluorescent imaging in centimeter-deep tissue possible [37]. Red/NIR region is suitable for deep *in-vivo* imaging , as water and hemoglobin have their lowest absorption, while tissue auto-fluorescence and scattering are relatively low [38],[37],[39],[40]. Despite the advantages that red/NIR imaging confers, there are limited number of fluorescent dyes with excitation and emission in this region. Indocyanine green (ICG) from the family of cyanine dyes, remains the only FDA-approved dye currently administered for clinical applications [37].

Environment-sensitive fluorescent probes are capable of responding to the changes in the immediate micro-environment. By changing emission characteristics in response to stimuli or cellular conditions such as polarity, pH, viscosity, hypoxia, ions etc. [41], [42] these probes often forewarn of a severe disease , e.g. higher blood viscosity in diabetic patients [41], [43] and lower pH and hypoxia in the tumor tissue of cancer patients [44].

Amongst the environmental stimuli, polarity is an important stimulus associated with hydrophobicity of proteins and consequently a broad range of diseases such as Alzheimer's, in which elevation of hydrophobicity is concurrent with the increase in aggregation-prone proteins [45]. In addition to conveying vital information about the degree of aggregation of proteins, polarity sensitive fluorescent probes have major applications in the synthesis of thermo-sensitive switches in conjunction with thermo-sensitive polymers (Figure 3.1).

Although direct thermometry with the use of temperature-sensitive fluorescent probes,

has been desired for its numerous applications, it has been fraught with obstacles. Rhodamine-B, a widely used probe for thermometry, has a mild thermo-sensitivity of 2.3% per degree Kelvin [46].

Multi-color methods, on the other hand, have not reached sensitivities of more than 10% [46]. Polarity sensitive fluorescent probes, in contrast, show a dramatic change in fluorescence emission strength in response to the change in polarity.

Recently a new polarity sensitive dye was introduced and its characteristics and application as a switchable fluorescent probe (SFP) were studied, when incorporated inside polymeric nanoparticles [47].

In this system the heat generated from the high-intensity focused ultrasound (HIFU) would increase the temperature of the tissue at the focus of the ultrasound above the lower critical solution temperature (LCST) of the probes, and elicit response from the thermo-responsive polymer. The shrinkage of the nanoparticle would affect its water content and consequently decrease the polarity of the immediate micro-environment of the fluorophores. This would trigger the fluorophore molecules to switch from an “OFF” or dark state at which they emit weakly to an “ON” state at which they emit strongly.

In pursuit of more versatile and stronger environment sensitive probes, herein, a set of aza-BODIPY-based and structurally-related fluorophores were investigated, their polarity and/or viscosity sensitivity and the structural characteristics leading to such behavior were explored.

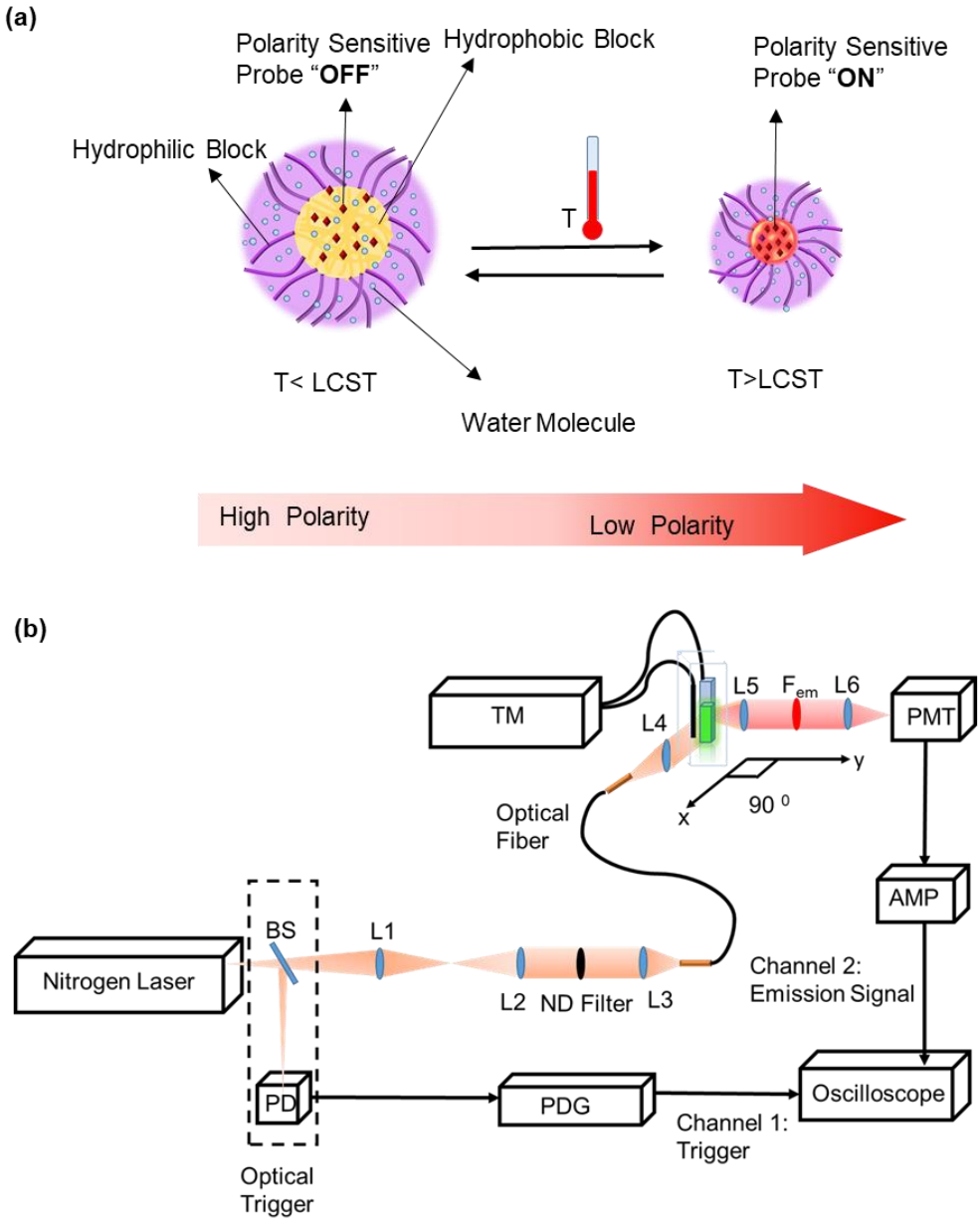

Figure 3. 1 (a) Nanoparticles made of thermo-responsive polymers, embedded with polarity-sensitive fluorophores, respond to the increase in temperature. By shrinking and excreting the water from the core of the nanoparticles, polarity is significantly decreased and polarity sensitive fluorophores switch "ON". (b) A schematic of the optical system.

3.2 Materials and Methods

3. 2. 1 Fluorescence measurement system: The fluorescence measurement system utilized for lifetime and intensity measurements was discussed in a previous work [14], [15] and in chapter 1, with minor changes to accommodate the temperature control system and corresponding filters for different fluorescent dyes. Briefly a combined laser system from Optical Building Blocks Corporation (Birmingham, New Jersey) generated an 800 ps pulse at the excitation wavelength of each dye. All lenses used in the system, except the band-pass filters, were purchased from Thorlabs Inc. (Newton, New Jersey). A pulse delay generator (PDG, DG645, Stanford Research Systems, CA) triggered the 2.5 GHz oscilloscope (DPO 7254, Tektronix, Beaveton, Oregon). The sample was loaded into a quartz cuvette (Starna Cells, Atascadero, CA) and the generated fluorescence light passed through a converging lens, the corresponding band-pass filter (BP, FF01-711/25-25 or FF01-785/62-25, Semrock, Semrock, New York). The emitted fluorescent light, was detected by a photomultiplier tube (PMT, H10721-20, Hamamatsu, Japan).The output of the PMT was converted to a voltage signal and was amplified by a broadband preamplifier (C5594, bandwidth from 50 kHz to 1.5 GHz, Hamamatsu, Japan). The signal was ultimately acquired by the multichannel, broadband oscilloscope. Each emission decay pulse recorded from the oscilloscope used for calculating fluorescence lifetime was an average over 100 excitation events. A temperature controller (PTC10, Stanford Research System, Sunnyvale, CA) was used to control the temperature. (Scheme 1).

3.2.2 Fluorescent emission strength and lifetime measurement: For lifetime calculations the acquired signal and the impulse response function were deconvolved and the decay curve was fitted to a mono-exponential decay function. Calculations were done using MATLAB (Natick, Massachusetts), with an iterative method to find the best fit with lowest residue. The maximum height of the decay curve was chosen as the peak emission strength[15]. For comparisons regarding the fluorophore-encapsulated Pluronic nano-particles a two-tail t-test

was conducted.

3.2.3 Response to Polarity: Fluorescent lifetime and strength of the emission of fluorophores were measured in different solvents. Solvents were obtained from Sigma-Aldrich Corporate (St. Louis, MO, USA), if not otherwise stated. Characteristics of the solvents used is provided in Table 3. 1.

Table 3. 1 Solvent properties.[48], [49].

Solvent	Solvent Type	$E_T(30)$ (kcal/mol)
Water	Polar protic	62.8
DMSO	Dipolar aprotic	45.1
1,2-dichloroethane	Polar aprotic	41.3
1,4-dioxane	Nonpolar	36
Toluene	Nonpolar	33.9
Glycerol	Polar protic	57
Ethylene Glycol	Polar protic	53.8

3.2.4. Response to Viscosity: To cover a range of viscosities, different mixtures of ethylene glycol (EG) with viscosity of 0.0161 Pa.s [50] and glycerol(Gl) with viscosity 0.934 Pa.s at 25^0 C were prepared [51]. Solutions were prepared by mixing glycerol and ethylene glycol at different volume ratios, Gl/EG (v/v)% of (0/100)%, (8/92)%, (16/84)%, (25/75)%, (50,50)%, (75/25)%, (84/16)%, (92/8)%,and (100/0)%. The viscosity of the mixture (Table 3.2) was calculated from Eq. (1) [48]:

$$\ln \eta_{mix} = \sum_{i=1}^{2} Xi \,.\, \ln \eta_i \,, \qquad (1)$$

In which η_i is the viscosity of each component, Xi is the mole fraction calculated based on the density of glycerol (1.26 g/cm^3) and ethylene glycol (1.11 g/cm^3) and the volume fraction.

Table 3.2. Viscosities pertaining to Gl/EG (v/v) % solutions.

Glycerol X_i	0.0000	0.0623	0.1272	0.2032	0.4334	0.6965	0.8731	1.0000
η (m Pa. s)	16.115	20.760	27.008	36.772	93.645	272.48	558.21	934.07

3.2.4 Preparation of fluorophore-encapsulated Pluronic nano-particles: Nanoparticles were synthesized based on a revised protocol [52]. Pluronic F-127(PEO100-PPO65-PEO100) [53] obtained from Sigma-Aldrich (St. Louis, MO, USA), as well as Pluronic F-98(PEO118-PPO45-PEO118) [54] and Pluronic F-68(PEO80-PPO30-PEO80) [54] obtained from BASF (Florham Park, NJ, USA), were dissolved in deionized water at pH 8.5 in a 5% (w/v) ratio with stirring. The fluorophores and tetrabutylammonium iodide (TBAI) from Sigma-Aldrich (St. Louis, MO, USA) were dissolved with a molar ratio of 1:8 in 6 ml chloroform (Fisher Scientific, Pittsburgh, PA, USA) by sonication using a bath ultrasonic cleaner (Branson 1510, Branson Ultrasonic Corporation, Danbury, CT) and added drop-wise to 15 ml of the Pluronic solution while stirring at 1200 rpm. The sample was then sonicated with an XL-2020 probe-sonicator (Misonix, Farmingdale, NY) while the probe intensity was kept at ~5-5.5. The sample was then moved to a beaker covered by aluminum foil with generated holes and stirred at 200-300 rpm overnight to evaporate the chloroform (Final concentration of flurophore was kept at about 50 µM). Free polymer was removed by filtering with a (10,000 MWCO) Amicon ultra centrifugation filters (Merck Millipore, Billericia, MA, USA) and large particles and/or impurities were filtered by 0.45 µm membrane filters (Fisher Scientific, Pittsburgh, PA, USA). For filtering samples were diluted 5 times, were centrifuged at 4500 G with a Legend X1 centrifuge (Sorvall™ Legend™ X1, Thermo, Marietta, OH), reduced and then brought back to the initial concentration. All measurements were done with filtered 1% samples, except for studying the effect of filtration where 1% and 0.2% samples, with and without filtering were prepared.

3.2.5 Fluorophore characteristics: The optical properties of six aza-BODIPY-based and structurally-related fluorophores were investigated in regards to their structure provided in Figure 3.2. All the fluorophores were kindly provided by The University of North Texas courtesy of Dr. D'asouza's lab. The synthesis methods for most of the fluorophores have been reported previously [55], [56], [38], [57].

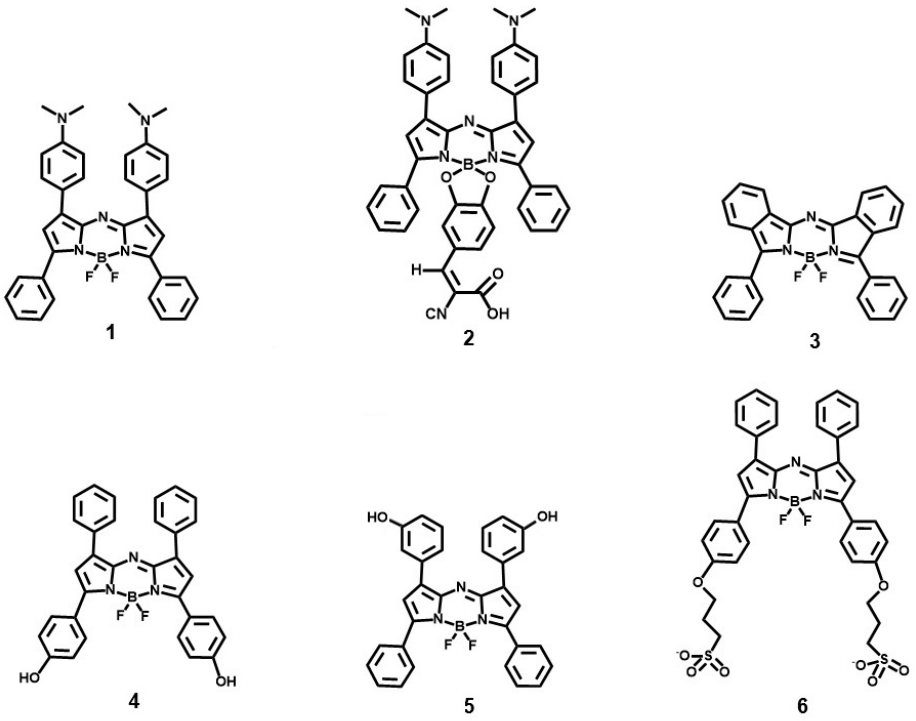

Figure 3. 2 Structure of the aza-BODIPY-based and structurally-related fluorescent dyes.

In the experiments that followed dyes were excited by their corresponding excitation wavelength (λ_{ex}), while the fluorescence emission (λ_{em}) was filtered by the Bandpass (BP) filter discussed in materials and methods (Table 3.3).

Table 3. 2 Summary of excitation and emission properties followed in experiments [38], [53], [54], [55].

Dye	Compound Name	Abbrev. Name	λ_{ex} (nm)	λ_{em} (nm)
1	Top Dimethyl amine ADPF2	TOP DMAADP	644	785/62 BP
2	Top Dimethyl amine ADPCNCA	TOP DMAADPCA	644	785/62 BP
3	Benzanulated ADPF2	Fused $ADPF_2$	710	785/62 BP
4	ADP $(OH)_2$ (Bottom)	ADP$(OH)_2$(Bottom)	655	711/25 BP
5	Top $(OH)_2$ ADP	Top $(OH)_2$ ADP	655	711/25 BP
6	ADP-Di Sulphonic acid	ADP DI(SA)	644	711/25 BP

3.3 Results

3.3.1. Response to Polarity: The fluorescence strength and lifetime of the fluorophores were measured in different solvents. By changing the solvents, the polarity of the microenvironment changed 28.9 units of polarity index, (E_T (30)) [58] (molar electronic transition energy of the negatively solvatochromic pyridinium N-phenolate betaine dye as probe molecule) measured in kilocalories per mole (kcal mol^{-1}) at room temperature (25 ^{0}C) and normal pressure (1 bar). The peak emission strength vs. polarity index is plotted in Figure 3.3. The maximum emission peak in all solvents is referred to as I_{max} and the emission peak in water is denoted as I_{water} with the lowest signal strength. In general the fluorescence emission strength of all the fluorophores, increased with decreasing the polarity.

As demonstrated in Figure 3.3, ADP(OH)2 Bottom, (i.e. fluorophore **4**), had the strongest dependency on the polarity with I_{max} to I_{water} ratio of ~ 4500, followed by Top Dimethyl amine ADPCNCA (TOP DMAADPCA), (i.e. fluorophore **2**), with a ratio of ~2000. ADP Di Sulphonic acid (ADP Di(SA)), (i.e. fluorophore **6**) , and Top $(OH)_2$ ADP, (i.e. fluorophore **5**), showed dependence on the polarity of the environment with I_{max} to I_{water} ratio of 370, and 260 respectively. Benzanulated ADPF2, (i.e. fluorophore **3**), showed some sensitivity to the polarity with I_{max} to I_{water} ratio of ~ 18, as well as Top Dimethyl amine $ADPF_2$ (TOP DMA ADP), (i.e. fluorophore **1**), with an I_{max} to I_{water} ratio of ~ 14 times. The previous report on this dye reported polarity sensitivity between 677 and 692 nm, while existence of a low intensity emission ranging from 795 to 822 nm was also reported[55]. Because of the particular interest in the red/NIR regeion, the polarity sensitivity, was measured between 725nm and 845nm.

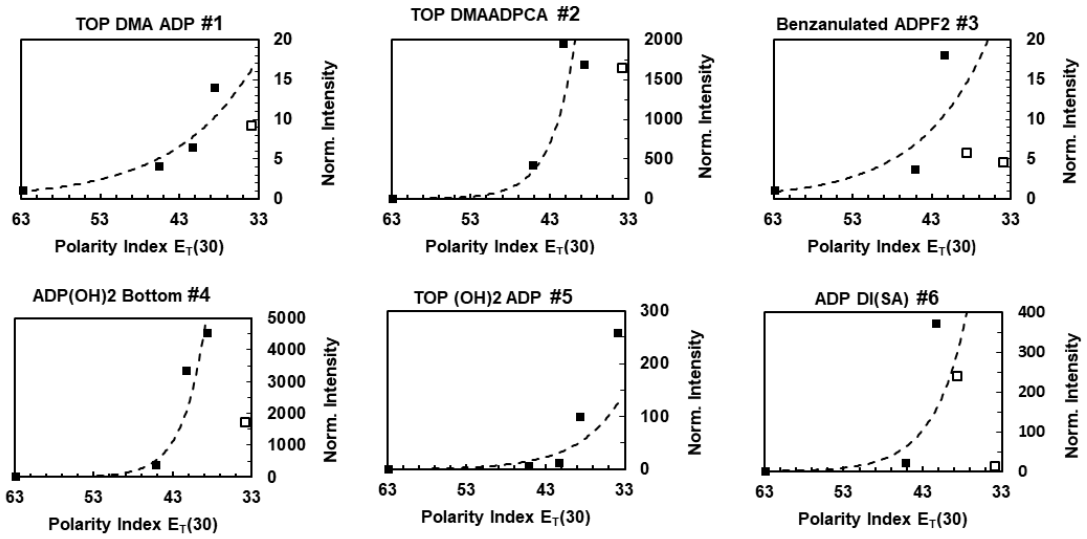

Figure 3. 3 Peak emission strength vs. solvent polarity. Exponential curve fitted to the points depicted with black squares.

It is worth mentioning that, the solubility of the dyes tested, are different, which might have affected the results to some degree. The decrease in the signal intensity from the highest value, observed for fluorophores **1**, **2**, and **4** in toluene(Last square), and for **3** and **6** in toluene and **1**, 4-dioxane (penultimate square) might be due to lower solubility in highly non-polar solvents.

The lifetime measurements revealed that the lifetime of fluorophores **2** and **3**, increased from 0.8 ns to 3.1 ns and from 2.67 ns to 5.03 ns respectively, while it just changed negligibly for fluorophore **1**(0.63 to 1.08 ns), fluorophore **4**(2.17 to 2.96 ns), fluorophore **5**(2.76 to 2.12 ns), and fluorophore **6**(2.36 to 2.47 ns) while polarity was changed from 62.8 to 33.9 based on E_T (30) units.

3.3.2 Response to viscosity: Measuring the response of the fluorophores to viscosity is important for delineating the mechanism by which the dyes respond to the environment. Here, the fluorescence strength and lifetime of the fluorophores were measured in regards to the viscosity of the environment while polarity was kept relatively constant (below 3.2 units of E_T

(30)). To quantitatively investigate the relationship between the fluorescence strength and lifetime with the viscosity, Förster-Hoffmann equation was used [59], [60]:

$$\text{Log } I = C + X \log \eta \quad (2)$$

Here, I is the peak emission strength, η is the solvent viscosity, C is a constant related to temperature and concentration and X a constant related to dye properties. For each fluorophore the logarithm of signal peak in ethylene glycol (lowest viscosity) was normalized to 1. As evident from the graphs (Figure 3.4), the fluorescence strength of fluorophores **2**, **4**, **5**, and **6** is relatively insensitive to viscosity. The Intensity of ADP BF_2, (i.e. fluorophore **3)**, dropped in the viscous medium with an I_{vis} to I_{non} ratio of ~ 0.003. Intensity of fluorophore **1**, increased for the initial points, for about 14 times at the beginning and then decreased. Lifetime of none of the probes changed significantly in response to viscosity.

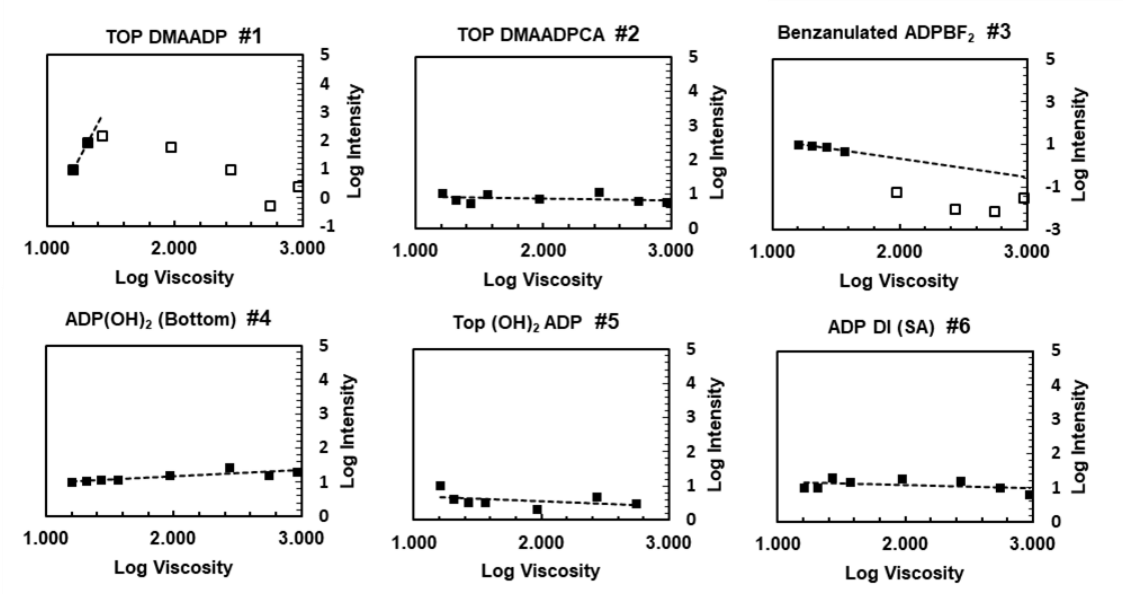

Figure 3. 4 Fluorescence strength in response to the change in the viscosity.

3.3.4 Fluorophore encapsulation in Pluronic nanoparticles: Based on the polarity sensitivity experiments, attachment of amine groups to the fluorophore was not necessary for having strong polarity-sensitive probes. Evidently, fluorophore **2** has a stronger fluorescence

strength compared to fluorophore **1** despite sharing the amine group in the same position (This is also correct considering the other emission band of 1 at 650-700 nm). Thus the response of fluorophores **4**, **5** and **6** all with substitutions of electron-donating groups to the aryl rings attached to the core of the fluorophore was investigated. Fluorophores were incorporated inside pluronic F-127 nanoparticles and the response to temperature was measured by changing the temperature in 3^0 C increments (Figure 3.5).

The response of fluorophore **4**, while incorporated inside pluronic F-127, F-98, and F-68 nanoparticles was also investigated. By increasing the temperature nanoparticles pass through two phases of shrinkage, the slow phase in which the polarity of the micro-environment surrounding the fluorophore is decreased at a very slow rate before the LCST (black arrow) and the fast rate at which the polarity decreases at a much faster rate and consequently the fluorescent strength increases. After reaching the first local maximum, the fluorescent strength reaches a plateau (red arrow), after which it either oscillates or remains constant. If the decrease in polarity and the increase in fluorescent strength is large enough and over a narrow range of temperatures, the pluronic-dye system can acts a switch, in which the switch is “Off” before or right at the LCST and “On” at or after the first maximum.

Although calculating I_{On} to I_{Off} ratio is arbitrary due to the existence of the slow increase phase, two methods for such a calculation is proposed: The Edge method in which the intensity of the first local maximum is divided by the intensity at the LCST, and the Vicinity method in which the intensity of the first local maximum is divided by the intensity of the point at the vicinity of the LCST. The temperature range between the first local maximum and the LCST is regarded as the transition bandwidth.

As shown in Figure 3.5, Pluronic F-127 with fluorophores **4** and **5** both act as a switch with an I_{On}/I_{Off} of 46.6 times and 7.07 times respectively (Edge method), both with a bandwidth of 6 degrees (Table 3.4). F-127 nanoparticle system with flurophore **6**, however, has an I_{On}/I_{Off}

of 4.71 times, over a wide bandwidth of 15 degrees that isn't suitable for applications that require switching mechanism. Based on these results Pluronic F-68 elicits a higher change in polarity of the microenvironment surrounding dye 4, compared to F-127 , with an I_{On}/I_{Off} of 117.02 times as opposed to 46.68 times.

This is directly related to the length of the hydrophobic chain of the Pluronic tri-block copolymers with the highest fluorescence strength pertaining to F-68 with the lowest hydrophobic chain of only 30 PO units.

Table 3.4 Summary of switching properties of Pluronic nanoparticles.

Pluronic Nano-particles	I_{On}/I_{Off} Edge Method	I_{On}/I_{Off} Vicinity Method	LCST	Bandwidth (^{0}C)
F-127_#4	46.6±2.01	145.74±25.08	25	6
F-127_#5	7.07±0.11	16.76±4.03	25	6
F-127_#6	4.71±1.11	9.62±3.81	13	15
F-98_#4	77.70±14.94	256.28±10.80	34	6
F-68_#4	117.02±10.14	233.46±46.35	61	9

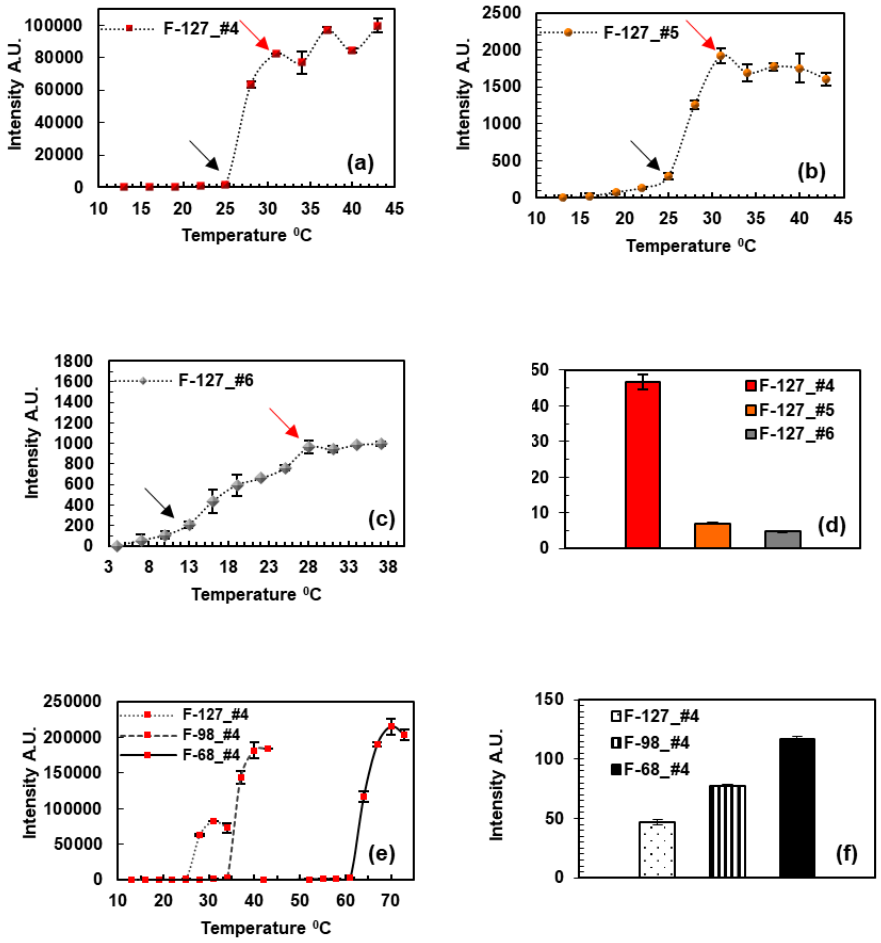

Figure 3. 5 Response of Pluronic F-127 loaded with fluorophores **4** (a), **5** (b), and **6** (c) to the change in temperature. Black arrows show the LCST and red arrows the first local maximum. (d) Pluronic F-127 nano-particles loaded with fluorophore **4** act as a very strong switch compared to nanoparticles of fluorophore **5** (P value of 0.0013). Both of the aforementioned nanoparticle/fluorophore systems act as a switch with narrow transition bandwidths. The Pluronic F-127 nanoparticles loaded with fluorophore 6 have a weaker fluorescence compared to nanoparticle/fluorophore system **4** (P value of 0.0015), while having a wide bandwidth excluding them as a switch despite being sensitive to polarity. There was no significant difference between nanoparticle/fluorophore systems 5 and 6 (P value=0.0966). (e), (f) Pluronic F-68 nanoparticles loaded with fluorophore **4** showed a stronger switching mechanism compared to Pluronic F-127 nanoparticles (P value of 0.0106).

3.3.4 Effect of filtration on LCST: The effect of filtration and dilution or lack thereof was studied on the LCST of the pluronic F-127 samples (Figure 3.6). 1% and 0.2% samples were chosen and their behavior was studied before and after filtration and dilution. Without filtration, monomers that didn't form micelles are still in the solution and contribute to the hydrophobicity of the microenvironment and hence LCST. Filtration on the other hand disposes most of these monomers and the polarity of the environment doesn't change much upon dilution and so the LCST remains the same.

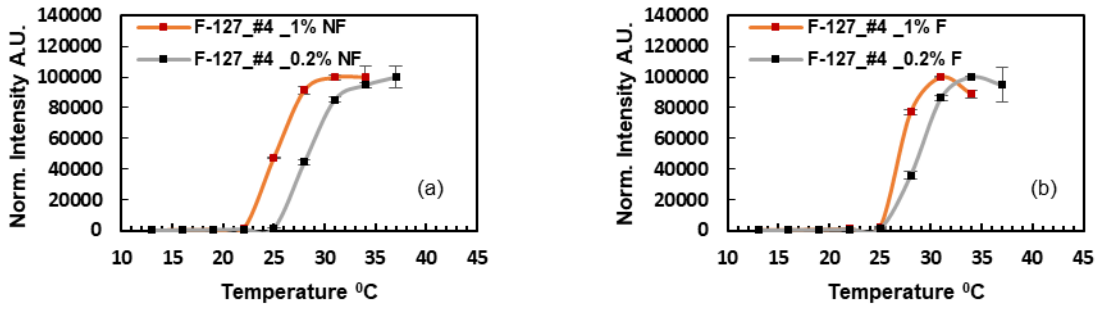

Figure 3. 6 The LCST of 1% non-filtered F-127 Pluronic nanoparticles loaded with fluorophore 4, is 3 degrees lower than the 0.2% (a). 1% and and 0.2% samples have the same LCST after filtration.

3.4 Discussion

Strong changes were observed in the fluorescence strength of fluorophores **2** and **4**, and moderate change in fluorophores **5** and **6** when decreasing the polarity, while a similar trend was observed, to a much lesser degree, for fluorophores **1** and **3**. The existence of amine groups attached to the fluorophore system seems unnecessary for having a strong polarity-sensitive probe. This is evident when comparing the structures of fluorophores **1** and **2**: Both of these

fluorophores have amine groups, but fluorophore **2** has a stronger polarity sensitivity. On a related note fluorophore **4** is a very sensitive probe despite not having an amine group. Based on these results substitution of electron-donating groups to the aryl rings attached to the core of the fluorophore in fluorophores **4**, **5** and **6** in conjunction with the Pluronic nanoparticles were further studied. Polarity sensitivity was most prominent when the hydroxyl groups were attached to the para position of aryls at 3- and 5- (Fluorophore **4**), and to a lesser degree when hydroxyl groups were attached to the meta position of the aryls at 1- and 7- (fluorophore **5**) or when the sulfonate groups were attached to the aryls at 3- and 5- positions (fluorophore **6**).

To act as a switch, fluorescence strength should increase over a narrow range of temperatures [47]. Despite the fact that fluorophores **4**, **5** and **6** are all polarity sensitive, only in F-127 Pluronic nanoparticles loaded with fluorophores **4** and **5**, the increase in signal takes place over a narrow temperature range, while in nanoparticles loaded with fluorophore **6**, the bandwidth is wide, thus excluding this system from being used as a switchable fluorescent probe. Fluorophore **6** however can be used in ratiometric measurements. The different behavior of fluorophore **6** might be due to its extreme hydrophilicity (only partially soluble in organic solvents such as chloroform), and the possible alteration of the microenvironment surrounding inside the fluorophore in Pluronic micelles.

Due to the complex and multivariate nature of the interaction of the fluorophores with the immediate microenvironment, it is not possible to confidently pinpoint a single factor responsible for the extreme change in fluorescence in response to the change in polarity. The observed significant decrease in fluorescence emission strength in polar solvents, considering the interconnected π-system of these fluorophores, can be due to specific solvent-fluorophore interactions such as “charge transfer pathways” which mainly include: photo-induced electron transfer (PeT), Internal charge transfer (ICT), or torsional intermolecular charge transfer (TITC).

The response of the fluorophores to the change in the viscosity of the microenvironment was measured for possible pathway delineation and also to estimate how freely the substitute

groups rotate, and the extent to which the absorbed energy is lost through rotational motion. It should be noted that although it was strived to keep the polarity constant while changing the viscosity, by changing the composition of the mixture, polarity changed 3.2 units of E_T (30), and inevitably the response to viscosity was convolved with the response to polarity.

As evident from Figure 3.4, for fluorophores **2**, **4**, **5**, **6** the signal intensity didn't change when viscosity was increased. Although this doesn't refute the fact that loss of energy due to rotational motion happens, it implies that such a loss is offset by the increase in fluorescence due to decrease in polarity when ET is the major constituent (lower viscosity and lower polarity with opposing effects). Contrarily to how fluorophores **2**, **4**, **5**, **6** behaved, fluorophores **1** and **3** showed a different response to viscosity. There is an increase in fluorescence strength for **1**, when the viscosity increases for the first initial points, followed by a curvilinear behavior with a decrease in fluorescence. For fluorophore **3**, the same curvilinear behavior takes place after the initial points with relatively constant signal. In **3**, in addition to the steric hindrance at 3- and 5- positions, the benzo rings are directly connected to the fluorophore, and therefore there is not much room for rotational motion around any of the bonds. Lack of response to viscosity, compounded by the decrease in fluorescent emission due the increase in polarity most probably leads to the decrease in fluorescence in fluorophores **1** and **3**. The obtained data is consistent with previously discussed research in the literature: phenyl substitutions at 3- and 5- position cannot rotate freely as a result of the steric hindrance caused by interaction of the hydrogen in the C-H bond with fluorine atom from the BF_2 [61], [62] and such substitutions would produce dyes that respond to the temperature and not the viscosity of the environment [63],[64]. Based on these results fluorescence strength measurement was superior to lifetime measurement is response to polarity.

3.5. Conclusion

Six members of the aza-BODIPY-based and structurally-related fluorophores with excitation and emission in the red/NIR region suitable for in vivo imaging, were investigated. It was shown that flurophores **2** and **4** were very strong polarity-sensitive probes, while fluorophores **5** and **6** showed relatively strong sensitivity. It was also shown that attaching amine groups to the fluorophore is not necessary for having strong polarity sensitive probes. After encapsulating the fluorophores **4**, **5** and **6** inside thermo-sensitive Pluronic nanoparticles, it was found that both fluorophores **4** and **5** can be used as ON-and-OFF fluorescence switches because of the dramatic change in peak emission fluorescence strength over a narrow range of temperatures. It was also shown that the signal intensity of Pluronic nanoparticles increases with decreasing the number of hydrophobic chains. As such these probes can be used as switchable fluorescent probes (SFPs). Another application of such dyes is the measurement of hydrophobicity of the proteins for structure elucidation analysis.

*** Acknowledgements: I want to thank Dr. Venugopal Bandi for synthesizing the environment sensitive probes and Dr. Francis D'Souza for collaborating with us.

Chapter 4

Developing pH-sensitive ultrasound switchable fluorescent probes

4.1 Introduction

Early cancer detection, while cancer is still localized and/or before it advances to a life threatening condition, might not only increase survival, but can also decrease morbidity, undue suffering and costs [65], [66]. Novel molecular imaging technologies with unprecedented depth and resolution are pivotal in early detection of cancer [66]. Reaching high sensitivities to differentiate cancer cells from healthy ones as early as possible remains the goal in the development of such imaging systems and probes [67].

The nature of ongoing accretion of mutations in cancers dictates the existence of a heterogeneous population within tumors. As such tumors usually contain populations of cells that differ by genotype [67], with 63 to 69% discrepancy in mutations of different regions of a somatic tumor [68]. Due to such level of heterogeneity it is very difficult, if not impossible, to develop probes that target a universal cancer biomarker.

Despite the heterogeneity in tumor cells, dysregulated pH is a hallmark of most cancers irrespective of their genetic origin [69]. While normal cells have an intracellular pH (pH_i) of about 7.2 and extracellular pH (pH_e) of 7.4, cancer cells have an elevated intracellular (pH_i) >7.4 and a low extracellular pH (pH_e) of 6.5-6.9 [69],[70] (Figure 4.1).

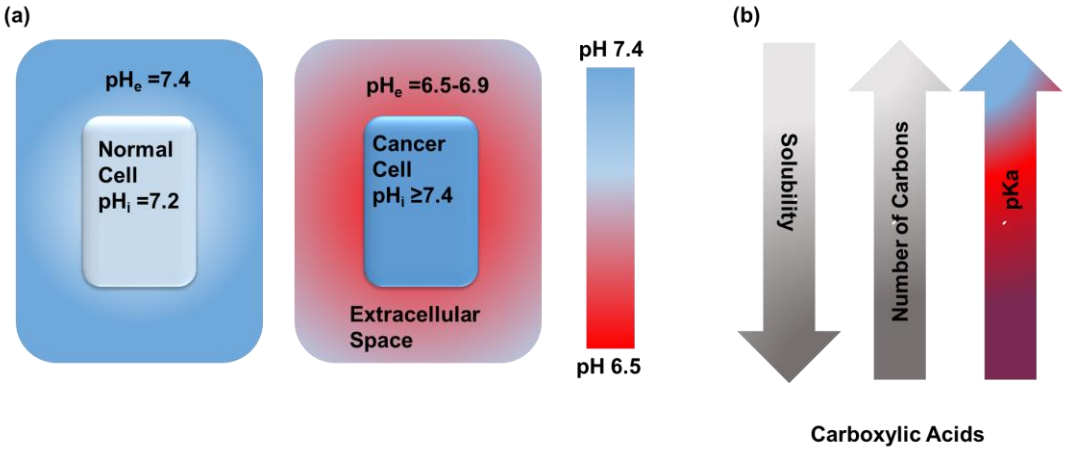

Figure 4. 1 (a) PH gradient in cancer cells is the reverse of normal cells with an extracellular pH of 6.5-6.9 in solid tumor cells [67], [68]. (b) The pKa of carboxylic acids increases with increasing the number of carbons while the solubility decreases with such an increase.

Literature is rife with pH-sensitive and dually pH/thermo-sensitive nanoparticles used for imaging and drug delivery, in which acrylic acid co-monomer has been used as a pH-sensitivity conferring agent in conjunction with a thermo-responsive polymer such as Poly (N-Isopropylacrylamide) (PNIPAm). This is despite the fact that the pKa of acrylic acid is 4.26 (at 25 °C), and the majority of the carboxyl groups are deprotonated between pH of 3-5. The sensitivity required for imaging solid tumors or for drug delivery is over pH 6.5, however.

Because of the narrow difference between the pH of tumor and healthy tissue (pH=~7.4) there is a need for carboxylic acid co-monomers with pKa values that are near the physiological pH to be used in the synthesis of thermo-responsive polymers. Although there are amines with pKa near 7.4 that can be used as pH sensitive co-monomers, their effect is not synergic with temperature. In the case of dually thermo- and pH-sensitive contrast agents for example, the temperature effect is to shrink the nanoparticles, and the desired effect is that the particles become swollen at physiological pH to suppress the effect of temperature. Amines, however, assume a positive charge below pKa and are neutral above their pKa which is against the effect

of temperature in polymers such as PNIPAm that shrink with temperatures above their LCST. For the case of thermo/pH-responsive nanoparticles with LCST polymers, the choice of acidic co-monomers remains the most viable choice. The pKa of carboxylic acids increases with increasing the number of carbons, as the longer chain acts as an electron donor to the carboxyl group which in turn decreases the acidity (Figure 4.1). The solubility of the carboxylic acids, nonetheless, decreases with increasing the number of carbons. From the members of the carboxylic acids having a double bound (at the farthest position), 8-nonenoic acid and 9-decenoic acid were still soluble for water-based reactions while 11-undecenoic was insoluble (The solubility of octanoic, nonanoic and decanoic acids had been previously discussed [71]).

Due to the addition of the water-soluble polarity-sensitive fluorophore during the reaction, water-based polymerization was followed for the ease of reaction and for protecting the fluorophore from harsh environment. From the carboxylic acids, 8-nonenoic acid and 9-decenoic were chosen as co-monomers of PNIPAm and compared to acrylic acid for pH sensitivity.

In this work a facile and fast method was developed for the synthesis pH-sensitive contrast agent based on (Poly N-isopropyl acrylamide) PNIPAm for USF imaging by revising existing protocols. In this system when the pH is below the pKa of the carboxylic acid, the carboxyl groups are protonated and neural. Upon applying a high intensity focused ultrasound (HIFU), the temperature increases inside the focal zone of the ultrasound transducer. Since the thermo-responsive polymer shrinks in response to the increase in temperature, the polarity sensitive dye that had a week fluorescence in the highly polar environment, now turns “ON” and emit a strong signal in the low polarity environment.

Contrary to the above scenario, when the pH is over the pKa of the acidic co-monomer, carboxyl groups start to deprotonate and as a result of the negative charge of the carboxyl group

the PNIPAm nanoparticles swell. At this swollen state the particles do not respond well to the change in temperature and so the particles don't completely shrink. As a result water is not expelled out fully and the polarity of the microenvironment doesn't decrease much and consequently the polarity sensitive dye, here indocyanine green (ICG), doesn't turn fully "ON", over the LCST of the nanoparticles. (Figure 4.2).

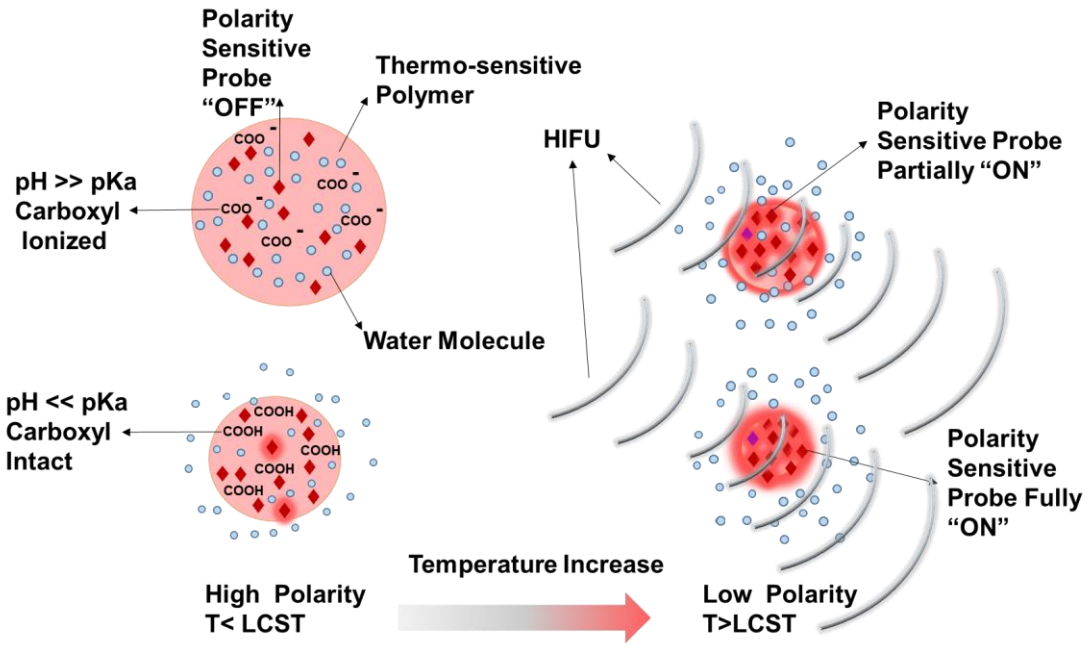

Figure 4. 2 USF imaging with pH sensitive contrast agents. Upon applying the HIFU, the temperature increase within the focal zone of the transducer. While at pHs lower than the pKa of the co-monomers, polarity sensitive probes turn "ON", at pH higher than the pKa, probes only partially turn "ON" depending on the pH due to partial shrinkage.

4.2 Materials and methods

4.2.1 Materials: N-Isopropylacrylamide (NIPAm), 4-4′-Azobis (4-cyanopentanoic acid) (ACA), 8-nonenoic acid and 9-decenoic acid were obtained from Sigma-Aldrich Corporate (St. Louis, MO, USA). Acrylic acid was obtained from Acros Organics. Triethylene Glycol Dimethacrylate was obtained from TCI (Tokyo, Japan). N, N′-Methylenebis (acrylamide) (BIS) was obtained from (Alfa Aesar Co., Inc.). Sodium dodecyl sulfate (SDS) was obtained from Fisher scientific.

4.2.3 Contrast agent development (ICG-encapsulated pH-sensitive PNIPAm nanoparticles): A revised protocol [72], [73] was used for the synthesis of NIPAm-based nanoparticles with acid co-monomer, in which NIPAm, (1 mole % based on NIPAm) of BIS, and variable amount of SDS (~5 mole% in (Series 1) S1, ~3 mole% in S2 to control the size) were dissolved in 60 mL de-ionized water (DI water) in a 250 mL Schlenk tube, followed by nitrogen purging for 30 minutes. ICG (0.038 mole %), ACA (4.4 mole %) and the corresponding amount of carboxylic acid as declared in each experiment were dissolved in mL of DI water and added to the tube. The tube was sealed and vacuumed until most bubbles were out and then purged with nitrogen (3 rounds). The reaction was carried out at 70 ^{0}C while stirring for 2 hours and dialyzed by a 10-kDa MWCO membrane. S2 samples were also filtered by a 10-kDa, Amicon ultra centrifugation filters (Merck Millipore, Billericia, MA, USA). Samples were lyophilized and rehydrated in BupH ™ Modified Dulbecco's Phosphate Buffered Saline (PBS) from Thermo Scientific (Rockford, IL, USA). (S1 samples had a concentration of 20 mg/mL and S2 3.3 mg/mL). S2 samples were then filtered by 0.45 µm membrane filters (Fisher Scientific, Pittsburgh, PA, USA) and the pH was adjusted by adding different concentrations of acrylic acid and allylamine in an effort to keep the total concentration and also the salt concentration of all the samples constant.

4.2.4 Fluorescent strength measurement in the cuvette system: A diode laser (MLL-FN-

808, 808 nm, Dragon Lasers, Changchun, Jilin, China) was used to illuminate the sample. The laser light was modulated at 10 KHz, 10 mV, with an offset of 700 mV with an Agilent function generator (33220A, Santa Clara, CA, USA). A qpod 2e temperature-controlled sample compartment with internal temperature controller from Quantum Northwest (Liberty Lake, WA) was used to hold the sample and regulate the temperature. T-App program from the same package was used for computer control. A Quiet One® Pro Series Aquarium Pump model 100 from Lifegard Aquatics (Cerritos, CA) was used for temperature control. A quartz cuvette containing 3 ml of the sample was inserted inside the compartment and the fluorescence emission light passed through a 830 nm longpass filter (BLP01-830R-25, Semrock, New York) before being detected by the spectrometer (Ocean Optics, Dunedin, FL, USA)(Figure 4.3 (d). For each sample fluorescence was measured two times and a one-tail paired t-test was conducted for comparison between the fluorescence strength at specific temperatures.

4.2.5 The USF imaging system: A USF imaging system has been recently developed based on an EMCCD camera [74] and was used for imaging the pH-sensitive contrast agent in a silicon phantom in this study. Briefly a function generator (33500B, Keysight Technologies, Santa Rosa, CA, USA) was used to generate a Vp-p of 50 mV, which was then amplified by a radio frequency power amplifier (A075, E&I, Rochester, NY, USA) with a gain of 50 dB, before being applied to a HIFU transducer (2.5 MHz, H-108, Sonic Concepts Inc., Bothell, Washington, USA). An 808 nm laser (MGL-II-808-2W, Dragon lasers, JL, China) was used to illuminate the sample after passing through a band pass filter (FF01-785/62-25, Semrock Inc., Rochester, NY, USA). A sample with a concentration of 3.33 mg/ml was injected to a silicone tube (ST 60-011-01, Helix Medical, Carpinteria, CA, USA) with an inner diameter of 0.31 mm and an outer diameter of 0.64 mm embedded at the edge of a clear silicone phantom (VST-50: VerSilTal Silicone Elastomer, Lakeside, AZ, USA).The background temperature was maintained at 27.5-28.5 ^{0}C and USF signals before and aftre the HIFU exposure were acquired.

4.2.6 USF Image Processing: The background image taken before firing the HIFU was

subtracted from the image taken after the HIFU was applied. A moving average filter was applied to average over 15 pixels along the x and y directions. Then, the averaged signal strength in an area consisting of 57 pixels in the x-direction and 54 pixels in the y-direction with the center at 565, 579 based on the FWHM of the image profile in the corresponding direction was calculated using MATLAB (Natick, Massachusetts)). Since the position of the phantom was fixed, this area was applied to all images. The FOV was 3x3 cm^2. One-tail t-test with equal variance was conducted for the USF image analysis.

4.3 Results and discussion

The fluorescence strength vs. pH was studied in S1 samples with increasing the temperature. The addition of co-monomers of acrylic acid, 8-nonenoic acid and 9-decenoic acid to the PNIPAm nanoparticles and the degree of acquired sensitivity to the pH change was investigated (Figure 4.3 (a), (b) and (c)). For comparing the pH sensitivity of the acidic co-monomers, ($I-I_{BG}$), defined as the fluorescence strength of the background when the probe was "Off" was subtracted from the fluorescence when the probe switched "On" (Figure 4.3 (e)). Based on these results, acrylic acid conferred little sensitivity to pH, especially between pH values 7.4 and 6.8, as there was no significant difference between the strength of the fluorescent signal at these two pH values at 41^0 C (P value=0.0835). On the other hand nanoparticles with co-monomers of both 8-nonenoic acid and 9-decenoic acids had significant difference between pH 7.4 and 6.8 at 41^0 C (P value=0.0266 and 0.0454 respectively). This data points out to the superiority of using acidic co-monomers with near physiological pKa for imaging and delivery purposes and accordingly 9-decenoic acid co-monomer was used as the pH-conferring agent for the rest of the experiments.

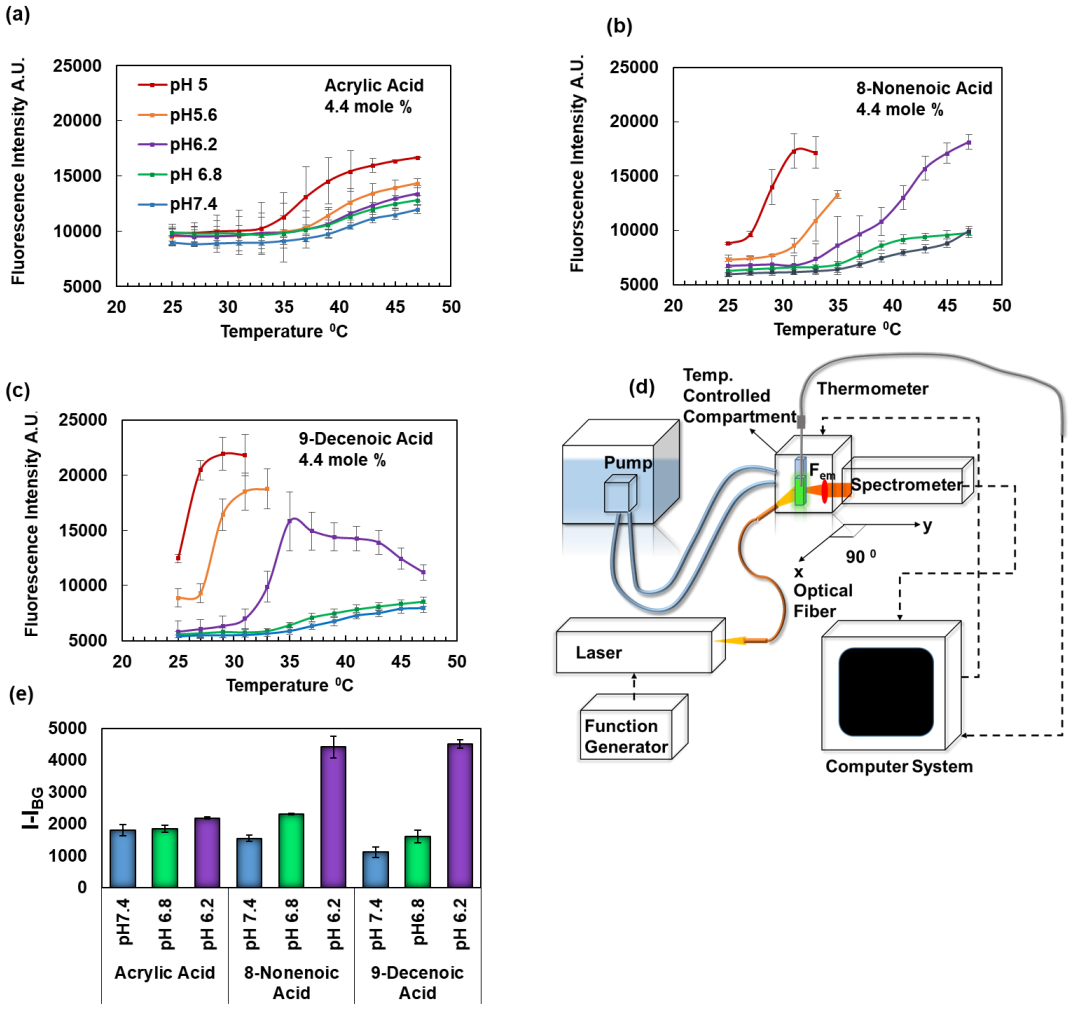

Figure 4. 3 Response of pH-sensitive USF contrast agents(S1) to temperature when (a) acrylic acid, (b) 8-nonenoic acid and (c) 9-decenoic acid were used as co-monomers with NIPAm (4.4 mole % of PNIPAm). 8-nonenoic acid and 9-decenoic acid co-monomers conferred better sensitivity to the change in pH in near physiological pH at 41^0 C compared to acrylic acid (P=0.026 and 0.045 respectively). (d) Schematic of the temperature-controlled fluorescent signal measurement cuvette system. (e) $I-I_{BG}$ was calculated at for (a), (b) and (c) at (43-37 ^{0} C), (41- 35 ^{0} C) and (39-33 ^{0} C) respectively. $I-I_{BG}$ was significantly increased between pH 7.4 and 6.8 for (b) and (c) (P-values 0.019 and 0.010 respectively.)

An important factor to study was the amount of carboxylic acid co-monomer ratio to the NIPAm monomers. USF contrast agents rely on thermo-sensitivity of the nanoparticles for the switching mechanism. The swelling due to the repulsion caused by the deprotonation of the acidic co-monomers, which is the heart of pH-sensitivity, however, counteracts the effect of temperature which is the shrinkage of the nanoparticles. Although this is favorable at physiological pH, the same effect at tumor pH would suppress the switching mechanism. In the S2 samples the amount of acidic co-monomers where changed from 2.94 mole% to 1.47 mole % to study this effect (Figure 4.4).

As apparent from the results thermo-sensitivity is preserved by using 1.47 mole % of the 9-decenoic acid co-monomers compared to a higher mole % of 2.94. On the other hand in the higher mole% the initial value of fluorescence increased with decreasing the pH, as opposed to the lower mole % sample in which the initial fluorescence is relatively the same among all samples.

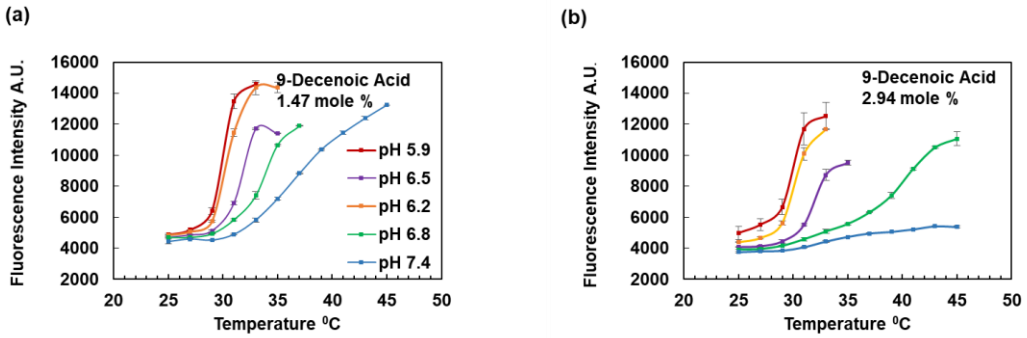

Figure 4. 4 Response of pH-sensitive contrast agents to temperature in 2 different percentage of acidic co-monomer. Thermo-sensitivity is preserved with the lower percentage of 9-decenoic acid co-monomers.

4.3.3 USF imaging: The USF signal strength in the area of HIFU exposure was compared among samples of S2 (PNIPAm/9-decenoic 1.47 mole %) with pH values changing from 5.9 to 7.4(Figure 4.4). This series was chosen based on the temperature curves in figure (4.4) and the fact that it provided the best trade-off between thermo-sensitivity and pH-sensitivity. The background temperature was kept at 27.5-28.5 ^{0}C as this series had a low LCST around this temperature. USF signal strength was calculated over an area of 2.64 mm^{2} (1.67 mm along X direction and 1.58 mm along Y direction) for all samples based on the FWHM of the image from sample at pH 5.9.

Based on the acquired results, USF signal strength significantly increased with the decrease of pH value from 7.4 to 5.9 with 0.3 unit decrements (P values provided in Figure 4.5). Accordingly the USF signal strength increased from 11.40 to 14.97(~ 31%) when pH was decreased from 7.4 (physiological pH) to 6.8 which is about the higher limit for tumor pH, and from 11.40 to 18.00 (~58%) when the pH decreased from 7.4 to 6.5.

This result demonstrates that this probe can be used for USF imaging and also the USF signal can be enhanced at low pH environment.

Although using 9-decenoic acid as the co-monomer conferred pH sensitivity near the physiological pH, it also decreased the LCST of the nanoparticles due to increasing the hydrophobicity, especially at lower pH values. A characteristic of the PNIPAm nanoparticles with acidic co-monomers is the tendency to for aggregation at high salt concentrations, low pH and high temperatures [75]. This happens when at a pH lower than the pKa of acidic co-monomer, most of the carboxyl groups are deprotonated and there is less repulsion to keep nanoparticles apart when temperature increases, and consequently nanoparticles become hydrophobic.

To mimick the physiological condition that is inherently a high salt condition, the samples in this work were all in prepared in PBS.

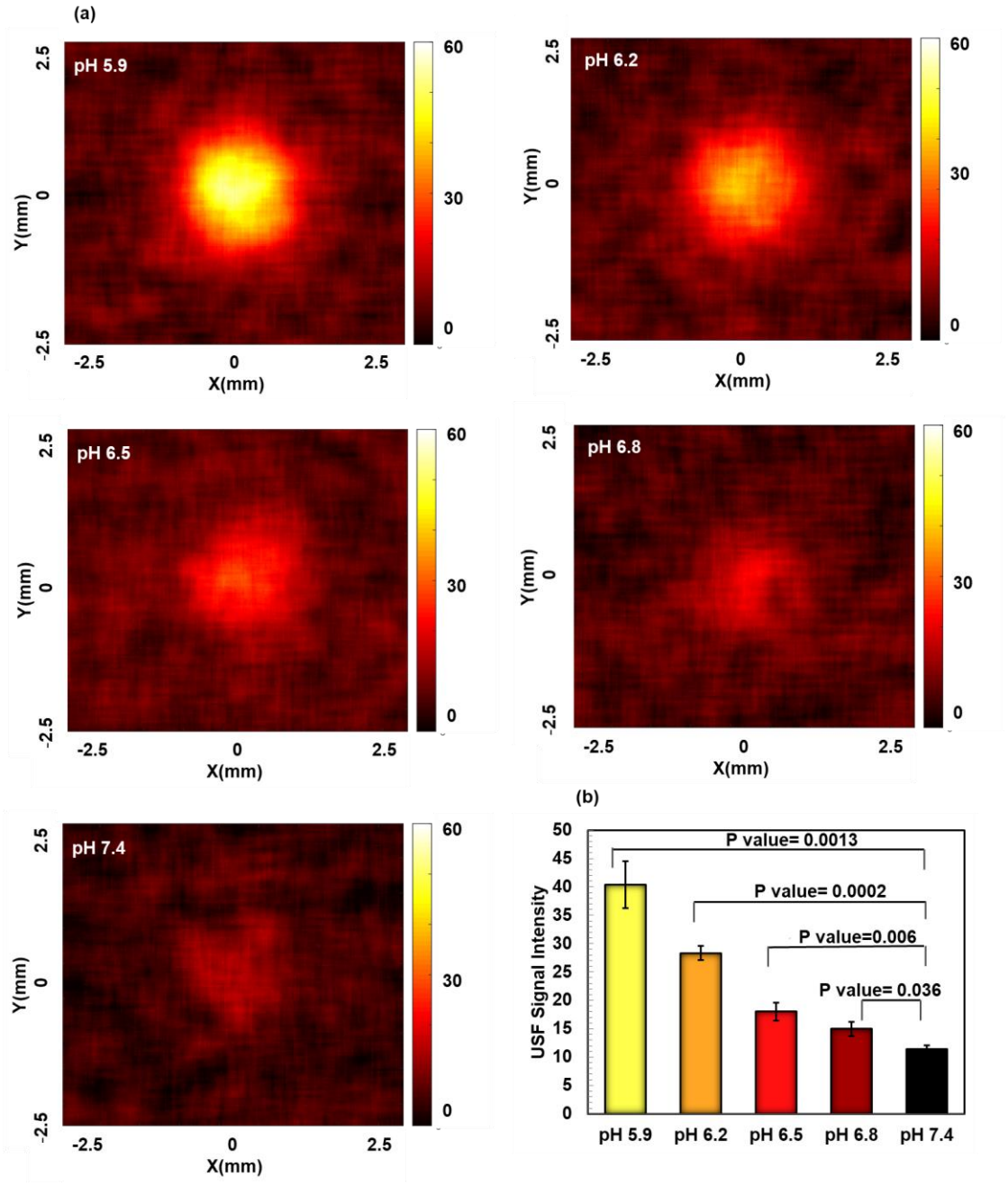

Figure 4. 5 USF signals of S2 samples of PNIPAM/9-decenoic (1.47 mole %) with pH 5.9 to 7.4. The background temperature was kept at 27.5-28 ^{0}C. The USF signal strength increased with decrease of the pH.

For counteracting the tendency of the nanoparticles to aggregate, a proposed method in the literature has been adding hydrophilic co-monomers such as PEG monomethyl ether monomethacrylate (PEG-MA)[73], or hydrophobic monomer (butyl methacrylate, BMA) [76] to the shell of the nanoparticles. As such these nanoparticles can be used at higher temperatures. Another method is increasing the LCST to near the body temperature at 37 ^{0}C, which is possible by addition of hydrophilic moieties to the nanoparticles.

4.4 Conclusion

A pH and thermo-sensitive USF contrast agent was synthesized by a facile and fast revised protocol. It was shown that 9-decenoic co-monomers grant pH sensitivity near the physiological pH, while, the widely used acrylic acid co-monomers are not able to grant pH sensitivity near the physiological pH. The limitation of the current generation of pH and thermo-sensitive USF contrast agent is low LCST that need to be improved.

Chapter 5

Conclusion

5.1 Sensitive USF contrast agents

Based on the results in chapters 2 and 3, ICT and PET pathways in the form of polarity sensitive dyes produce the maximum signal to background ratio. In such manner, polarity sensitive fluorophores surpass other methods such as FRET, especially when highly sensitive dyes discussed in chapter 3 such as NIR aza-BODIPY family is used in conjunction with thermo-sensitive polymers such as the the Pluronic family of polymers. Such a combination of highly sensitive fluorescent dyes and strong thermo-responsive polymers is capable of producing a signal to background ratio of over 100 times when temperature is changed within the safety limits.

5.2 PH-sensitive USF contrast agents

In chapter 4, a pH- and temperature-sensitive USF contrast agent was synthesized with sensitivity near the physiological pH. A revised facile and fast protocol was introduced that used the last soluble member of carboxylic acids 9-decenoic acid as a co-monomer for polymerization with NIPAm in a water-based reaction. This protocol can be easily used for producing pH/thermo-sensitive agents for imaging and also drug delivery purposes.

On a related note the superiority of using acidic co-monomer with pKa values that are near physiological pH and capable of granting pH-sensitivity at such pH values was shown. PNIPAm nanoparticles with 9-decenoic co-monomer had the ability to produce significant difference in signal strength even over very narrow ranges of pH (i.e. 7.4 and 6.8). As opposed to this result acrylic acid co-monomer which is vastly used as a pH-sensitive agent with its pKa

of 4.2, didn’t have the ability to confer such sensitivity near physiological pH.

References

[1] S. Wang, J. Lin, T. Wang, X. Chen, and P. Huang, “Recent Advances in Photoacoustic Imaging for Deep-Tissue Biomedical Applications,” *Theranostics*, vol. 6, no. 13, 2016.

[2] D. Gary and E. Kathryn, “Optical Imaging : Current Applications and Future Directions,” *J. Nucl. Med.*, vol. 49, no. 1, pp. 1–4, 2008.

[3] M. G. Muller, I. Georgakoudi, Q. Zhang, J. Wu, and M. S. Feld, “Intrinsic fluorescence spectroscopy in turbid media : disentangling effects of scattering and absorption,” vol. 40, no. 25, pp. 4633–4646, 2001.

[4] J. L. Sandell and T. C. Zhu, “A review of in-vivo optical properties of human tissues and its impact on PDT,” *J Biophotonics*, vol. 4, pp. 773–787, 2012.

[5] E. Hemmer, A. Benayas, F. Légaré, and F. Vetrone, “Exploiting the biological windows: current perspectives on fluorescent bioprobes emitting above 1000 nm,” *Nanoscale Horizons*, no. 1, pp. 168–184, 2016.

[6] M. Smith and M. C. Mancini, “Second window for in vivo imaging,” *Nat. Nanotechnol.*, vol. 4, no. 11, pp. 710–711, 2009.

[7] X. Dang *et al.*, “Deep-tissue optical imaging of near cellular-sized features,” *Sci. Rep.*, no. January, pp. 1–12, 2019.

[8] V. Wang, “Multiscale photoacoustic microscopy and computed tomography,” *Nat. Publ. Gr.*, vol. 3, no. 9, pp. 503–509, 2009.

[9] Envirocoustics, “Panametric_UT_Transducers.”

[10] J. KANDUKURI, “TECHNIQUES TO IMPROVE ULTRASOUND-SWITCHABLE

FLUORESCENCE IMAGING,” 2017.

[11] Y. Pei *et al.*, “High Resolution imaging beyond the acoustic diffraction limit in deep tissue via ultrasound-switchable NIR fluorescence,” *Sci. Rep.*, no. 1, pp. 1–7, 2014.

[12] A. You, M. A. Y. Be, and I. In, “Experimental characterization of temperature sensitive dyes for laser induced fluorescence thermometry,” vol. 074901, no. July, 2011.

[13] Y. Liu, J. A. Feshitan, M.-Y. Wei, M. A. Borden, and B. Yuan, “Ultrasound-modulated fluorescence based on microbubbles,” *J. Biomed. Opt.*, vol. 19, no. 8, p. 085005, 2014.

[14] B. Cheng *et al.*, “Development of Ultrasound-Switchable Fluorescence Imaging Contrast Agents Based on Thermosensitive Polymers and Nanoparticles,” vol. 20, no. 3, 2014.

[15] B. Saremi, M.-Y. Wei, Y. Liu, B. Cheng, and B. Yuan, “Re-evaluation of biotin-streptavidin conjugation in Förster resonance energy transfer applications,” *J. Biomed. Opt.*, vol. 19, no. 8, p. 085008, 2014.

[16] L. Stryer, “Fluorescence energy-transfer as a spectroscopic ruler,” *Annu. Rev. Biochem*, vol. 47, pp. 819–846, 1978.

[17] H. Sahoo, “Journal of Photochemistry and Photobiology C : Photochemistry Reviews Förster resonance energy transfer – A spectroscopic nanoruler : Principle and applications,” *"Journal Photochem. Photobiol. C Photochem. Rev.*, vol. 12, no. 1, pp. 20–30, 2011.

[18] W. R. Algar, A. J. Tavares, and U. J. Krull, “Analytica Chimica Acta Beyond labels : A review of the application of quantum dots as integrated components of assays , bioprobes , and biosensors utilizing optical transduction,” *Anal. Chim. Acta*, vol. 673,

no. 1, pp. 1–25, 2010.

[19] K. E. Sapsford, K. M. Tyner, B. J. Dair, J. R. Deschamps, and I. L. Medintz, “A Review of Current and Emerging Purification and Characterization Techniques,” *Anal Chem*, vol. 83, no. 12, pp. 4453–4488, 2011.

[20] E. R. Goldman and H. Mattoussi, “Quantum dot bioconjugates for imaging , labelling and sensing,” 2005.

[21] E. R. Goldman *et al.*, “Avidin: A Natural Bridge for Quantum Dot-Antibody Conjugates,” *J. Am. Chem. Soc.*, vol. 124, no. 22, pp. 6378–6382, 2002.

[22] D. S. Lidke *et al.*, “Quantum dot ligands provide new insights into erbB / HER receptor – mediated signal transduction,” vol. 22, no. 2, pp. 198–204, 2004.

[23] C. Zhang, H. Yeh, M. T. Kuroki, and T. Wang, “Single-quantum-dot-based DNA nanosensor,” vol. 4, no. November, 2005.

[24] R. Roy, S. Hohng, and T. Ha, “PRACTICAL GUIDE TO SINGLE- MOLECULE FRET,” *Nat. Methods*, vol. 5, no. 6, pp. 507–516, 2008.

[25] C. Zhang and L. W. Johnson, “Microfluidic Control of Fluorescence Resonance Energy Transfer : Breaking the FRET Limit **,” vol. 647, pp. 3482–3485, 2007.

[26] M. Levy, S. F. Cater, and A. D. Ellington, “Quantum-Dot Aptamer Beacons for the Detection of Proteins,” pp. 2163–2166, 2005.

[27] C. Zhang and L. W. Johnson, “Quantum-dot-based Nanosensor for RRE IIB RNA-Rev Peptide Interaction Assay,” *J Am Chem Soc.*, vol. 128, no. 16, pp. 5324–5325, 2006.

[28] M. C. Murphy, I. Rasnik, W. Cheng, T. M. Lohman, and T. Ha, “Probing Single-

Stranded DNA Conformational Flexibility Using Fluorescence Spectroscopy," vol. 86, no. April, pp. 2530–2537, 2004.

[29] H. Chen *et al.*, "Linked references are available on JSTOR for this article : Ionic strength-dependent persistence lengths of single-stranded RNA and DNA," vol. 109, no. 3, pp. 799–804, 2019.

[30] S. Hohng and T. Ha, "Single-Molecule Quantum-Dot Fluorescence Resonance Energy Transfer," vol. 61801, pp. 956–960, 2005.

[31] B. Kelly, J. R. Deschamps, and S. Buckout-White, "Quantum dot DNA bioconjugates: attachment chemistry strongly influences the resulting composite architecture," *ACS Nano*, vol. 4, no. 12, pp. 7253–7266, 2010.

[32] E. S. Gadelmawla, M. M. Koura, T. M. A. Maksoud, I. M. Elewa, and H. H. Soliman, "Roughness parameters," vol. 123, pp. 133–145, 2002.

[33] L. Technologies, "The Molecular Probes Handbook . A Guide to Fluorescent Probes and Labeling Technologies," vol. 76, no. 11, 2011.

[34] M. Hassan *et al.*, "Fluorescence Lifetime Imaging System for In Vivo Studies," vol. 6, no. 4, pp. 229–236, 2007.

[35] J. R. Lakowicz, *Principles of Fluorescence Spectroscopy*. New York: Springer, 2006.

[36] S. L. Shorte and F. Frischknecht, *Imaging Cellular and Molecular Biological Functions*. Berlin: Springer, 2007.

[37] R. Weissleder, "A clearer vision for in vivo imaging: Progress continues in the development of smaller, more penetrable probes for biological imaging," *Nat.*

Biotechnol., vol. 19, no. 4, pp. 316–317, 2001.

[38] M. Tasior, J. Murtagh, D. O. Frimannsson, S. O. McDonnell, and D. F. O'Shea, "Water-solubilised BF2-chelated tetraarylazadipyrromethenes," *Org. Biomol. Chem.*, vol. 8, no. 3, pp. 522–525, 2010.

[39] J. V. Frangioni, "In vivo near-infrared fluorescence imaging," *Curr. Opin. Chem. Biol.*, vol. 7, no. 5, pp. 626–634, 2003.

[40] H. Lu, J. MacK, Y. Yang, and Z. Shen, "Structural modification strategies for the rational design of red/NIR region BODIPYs," *Chem. Soc. Rev.*, vol. 43, no. 13, pp. 4778–4823, 2014.

[41] Z. Yang *et al.*, "Macro-/micro-environment-sensitive chemosensing and biological imaging," *Chem. Soc. Rev.*, vol. 43, no. 13, pp. 4563–4601, 2014.

[42] A. S. Klymchenko, "Solvatochromic and Fluorogenic Dyes as Environment-Sensitive Probes: Design and Biological Applications," *Acc. Chem. Res.*, vol. 50, no. 2, pp. 366–375, 2017.

[43] C. Irace, C. Carallo, F. Scavelli, M. S. De Franceschi, T. Esposito, and A. Gnasso, "Blood viscosity in subjects with normoglycemia and prediabetes," *Diabetes Care*, vol. 37, no. 2, pp. 488–492, 2014.

[44] Y. Kato *et al.*, "Acidic extracellular microenvironment and cancer," *Cancer Cell Int.*, vol. 13, no. 1, p. 1, 2013.

[45] M. J. Mitchell and M. R. King, "NIH Public Access," vol. 48, no. 1, pp. 1–23, 2014.

[46] C. E. Estrada-Pérez, Y. A. Hassan, and S. Tan, "Experimental characterization of

temperature sensitive dyes for laser induced fluorescence thermometry," *Rev. Sci. Instrum.*, vol. 82, no. 7, 2011.

[47] B. Cheng *et al.*, "The mechanisms and biomedical applications of an NIR BODIPY-based switchable fluorescent probe," *Int. J. Mol. Sci.*, vol. 18, no. 2, 2017.

[48] M. A. Haidekker, T. P. Brady, D. Lichlyter, and E. A. Theodorakis, "Effects of solvent polarity and solvent viscosity on the fluorescent properties of molecular rotors and related probes," *Bioorg. Chem.*, vol. 33, no. 6, pp. 415–425, 2005.

[49] "Web Services at the European Bioinformatics Institute."

[50] J. B. Segur and H. E. Oderstar, "Viscosity of Glycerol and Its Aqueous Solutions," *Ind. Eng. Chem.*, vol. 43, no. 9, pp. 2117–2120, 1951.

[51] "Viscosity, Surface Tension, Specific Density and Molecular Weight of Selected Liquids," *ACCU DYNE TEST*. .

[52] T. H. Kim, Y. Chen, C. W. Mount, W. R. Gombotz, X. Li, and S. H. Pun, "Evaluation of Temperature-Sensitive , Indocyanine Green- Encapsulating Micelles for Noninvasive Near-Infrared Tumor Imaging," pp. 1900–1913, 2010.

[53] A. Pitto-barry, N. P. E. Barry, and N. P. E. Barry, "Pluronic® block-copolymers in medicine: from chemical and biological versatility to rationalisation and clinical advances," *Polym. Chem.*, vol. 5, no. 10, pp. 3291–3297, 2014.

[54] C. Lee, H.-W. Tseng, P. Bahadur, and L.-J. Chen, "Synergistic Effect of Binary Mixed-Pluronic Systems on Temperature Dependent Self-assembly Process and Drug Solubility," *Polymers (Basel).*, vol. 10, no. 1, pp. 1–17, 2018.

[55] J. Killoran, S. O. McDonnell, J. F. Gallagher, and D. F. O'Shea, "A substituted BF2-chelated tetraarylazadipyrromethene as an intrinsic dual chemosensor in the 650-850 nm spectral range," *New J. Chem.*, vol. 32, no. 3, pp. 483–489, 2008.

[56] R. Gresser, M. Hummert, H. Hartmann, K. Leo, and M. Riede, "Synthesis and characterization of near-infrared absorbing benzannulated aza-BODIPY dyes," *Chem. - A Eur. J.*, vol. 17, no. 10, pp. 2939–2947, 2011.

[57] V. Bandi, M. E. El-Khouly, V. N. Nesterov, P. A. Karr, S. Fukuzumi, and F. D'Souza, "Self-Assembled via Metal − Ligand Coordination AzaBODIPY − Zinc Phthalocyanine and AzaBODIPY − Zinc Naphthalocyanine Conjugates: Synthesis, Structure, and Photoinduced Electron Transfer," *J. Phys. Chem. C*, vol. 117, no. 11, p. 5638−5649, 2013.

[58] C. Reichardt, "Solvatochromic Dyes as Solvent Polarity Indicators," *Chem. Rev.*, vol. 94, no. 8, pp. 2319–2358, 1994.

[59] D. Su, C. L. Teoh, N. Gao, Q. H. Xu, and Y. T. Chang, "A simple bodipy-based viscosity probe for imaging of cellular viscosity in live cells," *Sensors (Switzerland)*, vol. 16, no. 9, 2016.

[60] M. A. Haidekker and E. A. Theodorakis, "Environment-sensitive behavior of fluorescent molecular rotors," *J. Biol. Eng.*, vol. 4, pp. 1–14, 2010.

[61] X. Zhang, H. Yu, and Y. Xiao, "Replacing phenyl ring with thiophene: An approach to longer wavelength aza-dipyrromethene boron difluoride (Aza-BODIPY) dyes," *J. Org. Chem.*, vol. 77, no. 1, pp. 669–673, 2012.

[62] J. Chen, J. Reibenspies, A. Derecskei-Kovacs, and K. Burgess, "Through-space13C-

19F coupling can reveal conformations of modified BODIPY dyes," *Chem. Commun.*, no. 24, pp. 2501–2502, 1999.

[63] T. T. Vu, R. Méallet-Renault, G. Clavier, B. A. Trofimov, and M. K. Kuimova, "Tuning BODIPY molecular rotors into the red: Sensitivity to viscosity: Vs. temperature," *J. Mater. Chem. C*, vol. 4, no. 14, pp. 2828–2833, 2016.

[64] A. Vyšniauskas *et al.*, "Exploring viscosity, polarity and temperature sensitivity of BODIPY-based molecular rotors," *Phys. Chem. Chem. Phys.*, vol. 19, no. 37, pp. 25252–25259, 2017.

[65] "Early cancer diagnosis saves lives, cuts treatment costs," *World Health Organization*, 2017. [Online]. Available: https://www.who.int/news-room/detail/03-02-2017-early-cancer-diagnosis-saves-lives-cuts-treatment-costs. [Accessed: 03-Jul-2019].

[66] R. Etzioni *et al.*, "The case for early detection," *Nat. Rev. Cancer*, no. 3, pp. 243–252, 2003.

[67] D. Ling, M. J. Hackett, and T. Hyeon, "Cancer imaging: Lighting up tumours," *Nat. Publ. Gr.*, vol. 13, no. 2, pp. 122–124, 2014.

[68] D. Endesfelder *et al.*, "Intratumor Heterogeneity and Branched Evolution Revealed by Multiregion Sequencing," *new Engl. J.*, 2012.

[69] B. A. Webb, M. Chimenti, M. P. Jacobson, and D. L. Barber, "Dysregulated pH: a perfect storm for cancer progression," vol. 11, no. September, pp. 671–678, 2011.

[70] K. Zhou *et al.*, "Multicolored pH-Tunable and Activatable Fluorescence Nanoplatform Responsive to Physiologic pH Stimuli," 2012.

[71] H. C. Allen, B. A. Wellen, E. A. Lach, and H. C. Allen, “Surface pKa of octanoic, nonanoic, and decanoic fatty acids at the air–water interface: applications to atmospheric aerosol chemistry,” *Phys. Chem. Chem. Phys.*, vol. 19, no. 39, pp. 26551–26558, 2017.

[72] L. Jiang *et al.*, “Biomaterials pH / temperature sensitive magnetic nanogels conjugated with Cy5 . 5-labled lactoferrin for MR and fl uorescence imaging of glioma in rats,” *Biomaterials*, vol. 34, pp. 7418–7428, 2013.

[73] P. N. Core, S. Microgels, D. Gan, and L. A. Lyon, “Synthesis and Protein Adsorption Resistance of PEG-Modified,” *Macromolecules*, pp. 9634–9639, 2002.

[74] T. Yao, S. Yu, Y. Liu, and B. Yuan, “Ultrasound-Switchable Fluorescence Imaging via an EMCCD Camera and a Z-Scan Method,” *IEEE J. Sel. Top. Quantum Electron.*, vol. 25, no. 2, pp. 1–8, 2019.

[75] Z. H. Farooqi, H. Ullah, S. Mujtaba, and M. Siddiq, “Stability of poly (N-isopropylacrylamide-co-acrylic acid) polymer microgels under various conditions of temperature , pH and salt concentration,” *Arab. J. Chem.*, vol. 10, no. 3, pp. 329–335, 2017.

[76] D. Gan, L. A. Lyon, and R. V March, “Tunable Swelling Kinetics in Core - Shell Hydrogel Nanoparticles,” *J. Am. Chem. Soc.*, vol. 110, no. 21, pp. 7511–7517, 2001.

Biographical Information

Bahar received her Bachelor's degree in Physics from Amirkabir University of Technology. She got her Master's degree in Applied Physics from Texas Tech University. Her Master's thesis was regarding the synthesis of giant unilamellar vesicles (GUV) from RSE liposomes. She then joined Dr. Baohong Yuan's lab at the University of Texas at Arlington. During the course of her PhD studies she has worked on developing contrast agents for Ultrasound switchable fluorescence imaging. She has also worked on projects at University of Texas at Southwestern as a part of the joint biomedical engineering program.

She is the recipient of Carrizo & Utley fellowship, Provost's Level Graduate Teaching Fellowship, and Franklyn Alexander Scholarship. She has been a teaching assistant for courses such as ultrasound and optical imaging and bioinstrumentation